Extending the range of optically stimulated luminescence dating using vein-quartz and quartzite sedimentary pebbles

I. K. Bailiff[1], D. Bridgland[2] and Pedro P. Cunha[3]

(1) Department of Archaeology, Durham University, South Road, Durham DH1 3LE, U.K.
(2) Department of Geography, Durham University, South Road, Durham DH1 3LE, U.K.
(3) University of Coimbra, MARE - Marine and Environmental Sciences Centre, Department of Earth Sciences, Rua Sílvio Lima, Univ. Coimbra - Pólo II, 3030-790 Coimbra, Portugal

Highlights

- New approach to the dating of Quaternary sediments containing vein-quartz and quartzite pebbles
- OSL techniques applied to sliced pebble cores produce depth-dose profiles that are related to optical exposure history.
- Successful comparison of OSL ages with independently dated MIS 12, MIS 11, MIS 5 and Holocene depositional contexts.
- Low dose rates for vein-quartz and quartzite pebbles potentially enable further extension of the dating range.

Abstract

The feasibility of applying optically stimulated luminescence (OSL) techniques to obtain estimates of the burial age of lithic clasts in the form of pebbles of quartzose lithology is investigated in this study. We applied OSL measurement procedures to vein-quartz and quartzite pebbles from contexts at five sites with fluvial and coastal beach contexts of depositional age ranging from 500 ka to the mid Holocene. As in previous OSL studies with lithics, measured depth-dose profiles were interpreted to identify regions associated with key stages in the burial history of the pebbles, including the extent of pre-burial optical resetting, primary burial and any subsequent secondary stages of exposure to sunlight. While some of the pebbles had not been fully optically reset before burial, none were in field saturation, as commonly encountered with larger lithic clasts such as cobbles. The relatively low concentrations of radionuclides within vein-quartz and quartzite pebbles simplified the assessment of the radiation dose rate. OSL age estimates consistent with independent dating evidence were obtained for the three sites sampled in the UK (Langford Quarry, Leet Hill Quarry, Swanscombe Skull Site and Barnfield Pit) and one of two sites tested in Portugal (Forte Cão), whereas evidence of secondary optical bleaching detected in pebbles from a second site (Vale de Atela) underestimated the independent age for primary burial. The oldest depositional age of the contexts tested was ~500 ka (Leet Hill Quarry), and for some of the pebbles tested there was the capacity to extend the potential dating range further as the age equivalence of the limiting value of D_e was in excess of 1 Ma. The advantages of working with smaller, portable, clasts in the form of pebbles and with a lithology of higher transparency opens up a wide range of potential applications, whether the depositional processes are environmental or anthropogenic in origin or modification.

Keywords

Optically stimulated luminescence, dating, quartz, quartzite, pebbles, depositional processes, Pleistocene, Holocene

---

1. Introduction

Optically stimulated luminescence (OSL) techniques have been developed for dating depositional processes associated with a wide range of sedimentary contexts containing luminescent minerals, in particular granular quartz and potassic (Kf) feldspars contained within sands and finer components. These techniques have successfully provided reliable ages over a very wide chronological range, extending from the Middle Pleistocene to the late Holocene (Bateman, 2019). More recent developments have focused on the testing of lithic clasts of cobble size, including quartzite lithology (Simms et al., 2011, Sohbati et al., 2011; 2012a; King et al., 2019), where measurement of the variation of the equivalent dose with depth in the clast has formed a central part of the experimental technique. Such depth-dose profiles are used to identify the depth range within which optical resetting before burial had been sufficient, and to assess the suitability of the D_e values obtained for evaluation of the burial age. As the depth of optical penetration by sunlight in such cobbles is typically of the order of 10 mm, the inner volume is commonly found not to have been reset, giving rise to a saturation value of the OSL signal. Within the outer layers, the measured depth-dose profile obtained represents a complex combination of the effects of changes in the degree of optical resetting and the changing dose rate with depth. While the OSL characteristics of hyaline quartz (e.g., Sohbati et al., 2012a) or vein-quartz (Gliganic et al., 2019) have been found to be satisfactory for clasts from some sites, other studies (Huntley and Richards, 1997) have reported the finding of poor OSL characteristics with quartz, requiring the use of K-feldspar mineral extracts to determine the equivalent dose, D_e (Vafiadou et al., 2007; Guralnik et al., 2015; Simkins et al., 2016; Jenkins et al., 2018; Rades et al., 2018; Souza et al., 2019). In making a more detailed examination of the mineralogy of quartz, Simkins et al. (2016) attributed the poor sensitivity found with quartz extracted from Antarctic beach cobbles examined in their study to its limited quantity and variable crystal size occurring as anhedral intergrowths in feldspar, which gave rise to complications in dose rate assessment and a high overdispersion in D_e values. However, where the OSL characteristics of siliceous clasts are satisfactory, the low concentrations of lithogenic radionuclides generally found in the lithology of quartzite or vein quartz provide a potential advantage as the assessment of the dose rate is simplified. Depending on the relative radioactivity of the surrounding sediment, a reduction in the 'environmental' dose rate also potentially extends the maximum chronological range of the method. In this study we have examined whether these potential advantages can be exploited with pebble-sized clasts from a group of sites in fluvial and beach settings with independent age control, ranging in depositional age from Marine Isotope Stage 12 (MIS 12) to the Late Holocene. The pebble samples were obtained from five sites with Quaternary deposits, two in Portugal (Fig. 1a) and three in the UK (Fig. 1b) , further details of which are discussed in the following section.

2. Fieldwork

Samples of gravel were extracted under a large opaque plastic sheet erected to exclude sunlight from the sampling location. Following cleaning of the exposure under red light illumination, a cavity was excavated, into which a ~60 cm length of 110 mm diameter black PVC pipe was progressively introduced by removing sediment through the pipe until the tube reached an insertion depth of at least 50 cm. Further excavation beyond the inner end of the tube was performed to extract sediment, normally comprising gravel and coarse sand, which was promptly transferred to an opaque polymer storage bag. A scintillator probe was introduced into the sampling cavity following the extraction of samples to measure the gamma spectrum at the sampled location. The sampled contexts at each site are summarised below and further details are given in the Supplementary Material (Doc. 1).

2.1 Forte do Cão, Gelfa, Portugal

The Forte do Cão site is situated near the village of Gelfa, on the coast of NW mainland Portugal (Fig. 1a). The sampled site is located on the beach just north of the Forte do Cão fortress (Fig. 1a; geographic location: 41°47'47.25" N -8°52'15.26" W) at an elevation of 2.80 m above mean sea level (asl). Just above the modern beach sands and gravels, at an elevation of c. 2.40 m asl, lie the marine basal deposits of coastal terrace T5, and the OSL sample was taken from the gravels within in the exposure (Supplementary Material, Doc. 1, Fig. SM1.1a(i,ii); Fig. SM1.1b). The deposits within T5 are expected to have a burial age within the range 125-80 ka and, for the sample elevation given above, to have a depositional age of ~115 ka.

2.2 Vale de Atela, Alpiarça, Portugal

The Vale de Atela-east site (VAtela-E2) is located within the central mainland of Portugal, 2.5 km SSE of the municipality of Alpiarça (Fig. 1a). The sampled exposure is located (geographic location: 39° 14' 01'' N -8° 34' 03'' W; altitude, 32 m) in the valley of the Atela stream, which is a tributary of the Lower River Tagus (Tejo) (Supplementary Material, Doc. 1, Fig. SM1.2a(i, ii); Fig. SM1.2b). In this reach of the Tagus valley there is a terrace staircase with six levels. Amongst these, the Vale de Atela easternmost site contained in the fourth highest terrace, T4, has a significantly wider outcrop and is formed by considerably thicker sediments than the other terraces (e.g., Mozzi et al., 2000; Cunha et al., 2017). Its sedimentary sequence also shows internal complexity, with lower gravelly and upper finer-grained divisions dated by OSL to ~325–155 ka (Cunha et al., 2017). The lower division (Lower Gravels unit) which was sampled for this study in a disused gravel pit, was collected ~2.7 m below the top of the Lower Gravels unit and has a probable age of ~335–325 ka.

2.3 Swanscombe Skull Site and Barnfield Pit, Kent, UK

The site comprises the Swanscombe Skull Site National Nature Reserve (Barnfield Pit) located on the southern side of the Lower Thames valley in north Kent (Fig. 1b; geographic location: 51° 26' 39.40" N 000° 17' 47.79" E; Grid ref TQ 597 742). The site preserves a complex sedimentary sequence that has yielded rich assemblages of palaeontological and archaeological remains, notably Clactonian and Acheulian Palaeolithic assemblages (Bridgland, 1994; Bridgland et al., 2019). Within the site, the upper division of the Lower Gravel deposits from Phase I of the sequence assigned to MIS 11c (White et al., 2013) was accessed for sampling. The OSL sample was extracted from the upper 0.5 m of the Swanscombe Lower Gravel (Supplementary Material, Doc. 1, Fig. SM1.3a(i, ii); Fig. SM1.3b).

2.4 Leet Hill Quarry, Kirby Cane, Norfolk, UK

The Leet Hill site (Rose et al., 1999) is a sand and gravel quarry pit (Fig. 1b; geographic location: 52° 28' 59" N 001° 30' 18" E; National Grid Reference TM 380 869 3044) located ~15 km W of the East Anglian coast. The quarry has been cut into the N side of the Waveney valley and the exposures reveal deposits associated with the Anglian destruction of the Bytham River (Fig. 1b). Rising from the present floor of the quarry exposures is a sequence of sands and gravels corresponding to the Kirby Cane and Leet Hill sands and gravels of Bytham River origin, passing upwards into the Corton Sands, which represent MIS 12 glacial outwash. The Kirby Cane sands and gravels assigned were selected for OSL sampling (Supplementary Material, Doc. 1; Fig. SM1.4a(i, ii); Fig. SM1.4b). Although their age had been the subject of controversy, following detailed consideration of biostratigraphical evidence (Preece et al., 2009) and the reanalysis the of the Bytham terrace sequence in East Anglia (Westaway, 2009), they are dated to MIS 12.

2.5 Langford Quarry, Newark, Nottinghamshire, UK

Langford Quarry is located on the eastern flank of the modern floodplain of the River Trent ~8 km downstream from Newark upon Trent (Fig. 1b; geographic location: 53° 07' 57.58" N 000° 46' 33.01" W; National Grid Reference SK 8200 6020). Extraction of the sand and gravel

deposits had led to the recovery of archaeological finds, notably including late prehistoric human remains and Bronze Age metal artefacts (Howard et al., 2000; Howard, 2005; Bridgland et al., 2014). Dendrochronological dating of recovered tree remains within the sedimentary sequence indicated that the deposits had been significantly reworked and that the earliest tree remains dated to ~4500 BCE. The context from which the pebbles were sampled was within deposits underlying those that had yielded the redeposited archaeological remains (Supplementary Material, Doc. 1; Fig. SM1.5a(i, ii); Fig. SM1.5b).

3. Experimental

3.1 Sample preparation

The samples obtained from each site were examined and sorted in the laboratory under dim red illumination to identify pebbles of sufficient size with a visual appearance and texture resembling quartzite or vein quartz. The yield of potentially suitable pebbles of at least several cm (shortest dimension) varied according to site. Pebbles with a minimum dimension of ~2 cm were preferentially selected to enable cores extending between opposite surfaces to yield a sufficient number of (OSL) measurement slices (Supplementary Material, Doc. 2). The cores were extracted by drilling pebbles under water using a diamond faced core drill. Drills producing ~10.7 mm dia. cores were used with the larger pebbles and a smaller core drill (~8.5 mm dia.) drill was used with the smallest pebbles. Slices were cut from resin encapsulated cores using a 300 μm thickness diamond-faced wafering blade, with the cutting machine adjusted to produce slices of 700 μm thickness. In practice, the slice thickness varied between cutting sessions and was consequently measured after completion of OSL testing; the majority of slice thicknesses were within the range 600-750 μm. While the positioning the cut relative to the proximal surface of the core (during drilling) could be controlled, the same was not always available for the distal end, arising from core length and surface morphology of the distal end (Supplementary Material, Doc. 2). Measurement of the dose to the sub-surface region (i.e., < 2 mm) was confined to the first two of the sequence of cut slices (S1 and S2), where S1 incorporating the surface layer is referred to as the surface slice. Following removal of the encapsulation resin using a solvent, the slices were stored in dark libraries until required for measurement. In some cases, slices were further divided in half or quartered by fracturing using a surgical blade to enable different procedures to be applied at the same core depth. All operations were performed under dark or subdued red lighting conditions. Additional checks performed with beta-dosed cut slices stored in ambient (red) lighting conditions for 1 h indicated no significant loss of OSL signal.

3.2 Luminescence procedures

The luminescence measurements were performed using a Risø TL-DA-12 semi-automated reader (DTU Nutech, Denmark) containing a $^{90}Sr/^{90}Y$ beta radiation source installed in the irradiator. Optical stimulation of samples was performed using either 470 nm (~35 mW cm^{-2}) or 850 nm (~30 mW cm^{-2}) LEDs and the luminescence was detected after passing through a Hoya U-340 glass filter (7.5 mm). Core slices were mounted on stainless steel measurement discs that had been lightly coated with silicone oil. The dose rate to quartz slices from the $^{90}Sr/^{90}Y$ beta radiation source was calibrated (Supplementary Material. Doc. 3, Sec. 1) using slices that had been exposed to a known gamma dose (16.5 Gy) at a Secondary Standards Dosimetry Laboratory facility (Didcot, UK).

The equivalent dose, D_e, was determined by applying a single aliquot regenerative (SAR) procedure, similar to that described by Murray and Wintle (2000; 2003), but where the corrections for sensitivity change and thermal transfer were handled differently (Bailiff et al., 2014; Supplementary Material, Doc. 3, Sec.1). The test dose in the SAR protocol was replaced by a monitor dose comparable to the estimated natural dose; four levels of regenerative dose were applied to provide a range extending from one to four times the estimated natural dose. Although this dose range is sufficient for the

purposes of interpolation, estimates of the characteristic dose (Roberts and Duller, 2004), D_0, were also obtained with a small number of re-used slices to measure the dose response over an extended dose range. Dose recovery experiments were performed using two preheat temperatures (240 and 260 °C), with a third (280 °C) where sufficient slices were available to examine the dependence of the values of D_e on preheat temperature. The results of the dose recovery experiment were used to select preheat temperature(s) adopted in the SAR measurement procedure. The suitability of the latter was evaluated using the commonly applied rejection criteria (Supplementary Material, Doc. 3, Sec. 1), including tests for recycling and dose recovery (Wintle and Murray, 2006). Also, IR stimulation was applied at the end of each measurement sequence to test for IR bleaching and the presence of feldspar IRSL (Duller, 2003).

3.3 Dose rate assessment

The assessment of the dose rate due to lithogenic radionuclides within the pebbles and their burial media and was based on a combination of field and laboratory measurements. In situ measurements of the gamma ray spectrum at the sampled locations were performed using a calibrated portable gamma ray spectrometer (Supplementary Material, Doc. 3, Sec. 2). Portions of cored pebbles were extracted and analysed for parent ^{238}U, ^{232}Th and ^{39}K content using ICP-MS (Dept. Earth Sciences, Durham University). The average specific activities of detectable progeny of the ^{238}U and ^{232}Th decay chains and ^{40}K, in sediment and a selection of pebbles were measured using a high-resolution gamma spectrometer (Supplementary Material, Doc. 3, Sec. 3). The specific activities and concentrations were converted to infinite medium dose rates using the conversion factors calculated previously (Bailiff et al., 2014) and similar to those given in Guérin et al. (2011).

As discussed in the following section, the beta dose rate within the sub-surface region comprises two components, one due to external beta radiation from sources in the sediment that decreases with depth and the other from sources within the lithic that increases with depth beneath the surface. To calculate these two components as a function of depth for the depth range containing the first two slices (~2 mm) radiation transport simulations, were performed to calculate factors that relate the beta dose rate within volumes corresponding to the initial slices in a core (S1-S3; surface - ~3 mm depth) to the full energy release beta dose rate. The simulations were performed for each lithogenic source (^{40}K, nat. U and ^{232}Th) distributed a) in the sediment and b) in the lithic. Further details of the simulations are given the Supplementary Material (Doc. 3, Sec. 3). The data generated from these simulations were also used to calculate beta linear attenuation coefficients for use in the model illustrations discussed in the following section.

The cosmic dose rate was calculated for each sampled context using a simple model employing Prescott and Hutton's (1988; 1994) depth-dose data, which is comparable to the approach employed by Munyikwa (2000). The time-averaged cosmic dose rate during burial was calculated using this model, taking into account the development of overburden from primary burial to the present natural ground surface (in the absence of quarrying) on the basis of an interpretation of the site stratigraphy (Supplementary Material, Doc. 3, Sec. 3). It was assumed that any long-term variations in cosmic rate dose rate during the last 500 ka had not resulted in a significant deviation from the values calculated using Prescott and Hutton's formulae; a type B uncertainty of ±5% associated with the dose rate was included in the calculation of the overall uncertainty in the OSL age. However, it would be worthwhile reviewing of the most recent data on the fluctuations of geomagnetic field and galactic cosmic ray intensities (e.g., Erlykin and Wolfendale, 2010) to assess their potential effect on cosmic dose rate during the late Pleistocene.

4. Depth-dose profile models

The form of the depth-D_e profiles for pebbles is expected to differ in detail from those typically reported for cobble-sized lithic clasts (e.g., Sohbati et al., 2011). For quartzose pebbles that possess relatively higher internal optical transparency and prolonged exposure history, the extent of optical

bleaching or 'resetting' (removal of legacy trapped charge) due to pre-burial exposure to sunlight is likely to extend to greater depths (e.g., >10 mm) than is typically the case for granite cobbles, for example. Where the interior of a pebble-size clast is free of lithogenic radionuclides, the depth-D_e profile is expected to be approximately flat beyond a depth of ~2 mm (i.e., the maximum range of external beta radiation from lithogenic radionuclides) beneath the surface as the effect of the attenuation of gamma radiation over distances of a few cm is weak. As few lithics are free of lithogenic radionuclides, the form of the depth-D_e profile depends on their concentration and spatial distribution, but the profile is expected to be similarly flat where the distribution is effectively uniform. A version of a previously developed optical bleaching model for lithic clasts (Polikreti et al., 2002; Laskaris and Liritzis, 2011; Sohbati et al., 2011; Sohbati et al., 2012; Freiesleben et al., 2015), in the form of a semi-infinite slab of 20 mm thickness (h), was applied to illustrate (Fig. 2) the form of profiles for a hypothetical lithic pebble undergoing an alternating series of exposures and burials.

The following expressions are based on those developed by Sohbati et al (2012c) and Freiesleben et al. (2015) to describe the dependence of the luminescence signal, $L_n(x)$, with depth, x, in a semi-infinite slab of thickness h, during an alternating sequence of stages of exposure to light on both faces of the slab (Eqn 1; n=1, 3 and 5) and burial (Eqn 2; n= 2 and 4),

$$L_n(x) = L_{n-1}(x) \left[\frac{\{E(x)e^{-t(E(x)+F(x))}+F(x)\}}{E(x)+F(x)}\right] \left[\frac{\{E(x\prime)e^{-t(E(x\prime)+F(x\prime))}+F(x\prime)\}}{E(x\prime)+F(x\prime)}\right] \quad (1)$$

$$L_n(x) = (L_{n-1}(x) - 1)\, e^{-F(x)t} + 1 \quad (2)$$

where, x' = (h-x); L_0=1; E(x) = ($\overline{\sigma\varphi_0}\ e^{-\mu x}$) defines the rate of loss of trapped charge due to light exposure with depth (e.g., at the surface when x=0), representing an average obtained by integration over the incident optical spectrum (Sohbati et al., 2011); σ = photoionisation cross section (cm^{-2}), φ_0 = photon flux ($cm^{-2}\ s^{-1}$), t= time (s), μ= optical attenuation coefficient (mm^{-1}); F(x) = $\dot{D}(x)/D_0$, is the trap filling rate.

The function F(x) was evaluated at each depth, x, by calculating the total point dose rate, $\dot{D}(x)$, following a formulation based on that used by Freiesleben et al. (2015), given by,

$$\dot{D}(x) = {}_{lith}\dot{D}_{\beta}^{\infty}\ [1 - 0.5(e^{-b_l x} + e^{-b_l(h-x)})] + {}_{sed}\dot{D}_{\beta}^{\infty}\ [0.5(e^{-b_s x} + e^{-b_s(h-x)})] + {}_{sed}\dot{D}_{\gamma} + \dot{D}_{cos} \quad (3)$$

where, b_l and b_s are the beta linear attenuation coefficients (mm^{-1}) calculated for the radionuclide composition in the lithic and sediment media respectively (Table 1), $\dot{D}_{\beta}^{\infty}$ is the point absorber infinite medium beta dose rate and ${}_{sed}\dot{D}_{\gamma}$ and $\dot{D}_{cos}$ are the average effective gamma and cosmic dose rates, respectively, within the lithic volume. For the purposes of illustration of the model, the minor contribution of the effective alpha dose rate is not included in Eqn 3.

If the luminescence intensity, L, has the same proportionality to the absorbed dose throughout the medium, the dose response characteristic, given by

$$L = L_0\,(1 - e^{-D_e/D_0}), \quad (4)$$

can be rearranged as

$$\frac{D_e}{D_0} = -\ln\left(1 - \frac{L}{L_0'}\right), \quad (5)$$

where, D_e is the equivalent dose, L_0 is the saturation value of the luminescence intensity and D_0 is the characteristic dose, as measured in the laboratory, and L_0' the saturation value of the luminescence intensity during burial.

Substitution of values of $L_n(x)$ for L/L_0' in Eqn 5 enables the depth-luminescence profiles to be presented as depth-dose profiles, where the values of D_e are normalised to the characteristic dose, D_0. This provides a more direct comparison with experimental data where saturation values of the luminescence intensity are not obtained, as is the case for the pebble interiors examined in this study (although approaching saturation in the case of Leet Hill Pebble 4). When comparing measured with modelled profiles, it should be noted that, in the model, the opacity of the lithic is assumed to be uniform and that the dominant mechanism of any loss of trapped charge following primary burial is by optical exposure.

The depth-dose profiles calculated using the profile model with the parameter values listed in Table 1a,b are shown in Fig. 2 for three different burial histories set within a nominal total burial period of 500 ka. The profiles obtained after each light exposure and burial stage were calculated using a value of $\overline{\sigma\Phi_0}$ (6.34×10^{-9} s^{-1}) similar to that (6.7×10^{-9} s^{-1}) obtained by Sohbati et al. (2012) for a sandstone clast extracted from a known-age road cut exposure. It is worth noting that a significantly higher value of $\overline{\sigma\Phi_0}$ (5.9×10^{-6} s^{-1}) was evaluated by Gliganic et al. (2019) for a flake of relatively transparent quartzite produced in a stone tool quarry in southern Tibet, for which the exposure period was known. The profiles calculated using the higher value of effective detrapping rate are similar for exposure periods that are reduced proportionally (i.e., by 3 orders of magnitude, as indicated in the lower section of Table 1). This is of relevance to the history of individual pebbles which are, as mobile clasts in fluvial and coastal environments, likely to have undergone highly variable levels of incident direct or indirect sunlight during periods of exposure, giving rise to differences in the level of residual charge obtained following prolonged light exposure, as discussed further below. The values of the linear beta attenuation coefficients, b_l and b_s, used in the model calculations (Table 1b) are mean values of the coefficient calculated for each lithogenic source, weighted according to proportional beta dose rate contributions made by each radionuclide (^{40}K, nat. U and ^{232}Th) within the burial sediment (K(0.73); U(0.17); T(0.10)) and the lithic (K(0.08); U(0.14); Th(0.78) selected for the model illustration. The coefficient values are significantly higher than those used in the earlier cobble studies which were based on those given in Aitken (1985), but they are comparable to those presented in the detailed study by Riedesel and Autzen (2020) for granite cobbles. As a consequence, the form of the profile in the sub-surface region is much steeper than that shown in the earlier work.

Each of the numbered profiles (Fig. 2a-c) correspond to the stages of burial history indicated in Table 1a, commencing with the immediate post-burial condition (1), followed by one (History 1) or more (Histories 2 and 3) stages of light exposure and reburial for the periods as indicated in the table. In the case of History 1 (Fig. 2a), the period of pre-burial exposure (10 ka) is selected to produce a residual central peak (curve 1) that results from incomplete optical bleaching of charge in OSL traps before burial (referred to here as optical resetting). The profile developed after a burial period of 500 ka is represented by curve 2, where the residual central peak remains dominant and the effects of the higher beta dose rate in the outer layers are evident, producing a characteristic uplift in the profile at the interface with the burial medium. However, a relatively short period of light exposure (2 a) before the end of the burial period (e.g., contemporary disturbance) would remove that uplift, producing curve 3.

In History 2 (Fig. 2b) the duration of light exposure before primary burial of 500 ka minimises the trapped charge population in the central region (curve 1). At long exposure times a balance of charge trapping and optical detrapping is obtained and, for the lower optical detrapping rate selected ($\overline{\sigma\Phi_0}$ = 6.34×10^{-9} s^{-1}), this results in a calculated residual population of trapped charge (Sohbati et al., 2012c)

equivalent to a dose of 3.7% of D_0 (curve 1). If the higher rate ($\overline{\sigma\Phi_0}$ = 6.34 x 10^{-6} s^{-1}) is specified, a negligible residual population is obtained after an exposure of 250 a. The profile developed after a burial period of 180 ka is given by curve 2, when a second stage of optical exposure commences that progressively depletes trapped charge from the outer to the inner regions of the pebble, producing a broad peak (curve 3). After an exposure of 2 ka, the onset of trapped charge depletion at the central position is evident (by 5% in this case), and longer exposure causes a progressive narrowing of the peak accompanied by further reduction in trapped charge (e.g., 10% after 5 ka). Following an exposure of 2 ka, reburial for a further 320 ka results in the development of curve 4. If there were a final period of light exposure (2 a) before the end of the burial period, curve 5 is obtained.
The presence of a central peak in both History 1 and History 2 profiles, although of differing form in these two histories, indicates a potential ambiguity when interpreting the cause of a peak. That is, whether it should be attributed to partial resetting before burial, or, where optical resetting was complete or maximal, to a secondary episode of exposure and reburial that occurred at an intermediate stage during the total burial period. This issue is relevant to the interpretation of the profiles obtained with one of the Leet Hill pebbles.

History 3 is similar to History 2, but during the secondary stage of light exposure, light is incident only on one face (left hand) of the slab, which is equivalent to the model configured by Freiesleben et al. (2015). The (bi-directional) light exposure before primary burial is sufficient to obtain maximal depletion of trapped charge (curve 1) as in History 2. Following burial for 280 ka (curve 2), a secondary stage of light exposure depletes the trapped charge within the first ~12 mm depth (curve 3). Reburial for a further 220 ka results in curve 4. As with the other two histories, a final brief stage of (bi-directional) light exposure would deplete trapped charge in the outer regions of the pebble, producing curve 5.

Although these models are idealised, they provide a convenient starting point when interpreting the experimentally determined depth-D_e profiles. In the latter, regions in the profile containing multiple or single values of D_e interpreted to be associated with primary burial, secondary exposure and reburial or the presence of a peak, are denoted by 'A', 'B' and 'P', respectively. Other than using the model discussed above to predict general forms of profile, the fitting of calculated bleaching profiles to the experimental data with the aim of extracting quantitative values for the optical parameters in the above equations was not attempted. The results of recent work (Meyer et al., 2018; Gliganic et al., 2019) have shown that the optical and physical conditions within the lithic clasts and the illumination conditions are much more complex and varied than hitherto assumed in such calculations, requiring independent measurements of $\overline{\sigma\Phi_0}$ and μ (Ou et al., 2018).

5. Results

5.1 Equivalent dose determination

The number of potentially suitable pebbles (appearance of light colouration under red light; smooth surface and sufficient size) varied between the sites examined and, although the yields were generally low, this was in keeping with expectation based on previously published assessments of the sediment mineralogy for the sites sampled (Bridgland, et al., 2014; 1994; Cunha et al., 2017). From the five sites producing suitable pebbles, nine pebbles were sampled for D_e measurements. A total of 12 cores were extracted from these pebbles, yielding 200 slices; all except 24 slices exhibited OSL characteristics satisfactory for evaluation of D_e. Given the limited number of slices available from each core, some were split into segments, enabling both dose recovery experiments and determinations of D_e to be performed at the same core depth.

Following luminescence measurements, an examination of slices under cross-polarised light indicated that all three pebbles from Swanscombe and Pebble 3 from Leet Hill were derived from vein quartz

and that the remaining pebbles from Forte do Cão, Vale de Atela, Langford and Pebble 4 from Leet Hill had a quartzite structure. Images of slices obtained under reflected white fluorescent light illumination (Supplementary Material, Fig. SM2.2) provided a measure of their relative opacity, indicating that the slices of Leet Hill Pebbles 3 and 4 and Swanscombe Pebbles 2 and 8 were of relatively higher opacity and those of Forte do Cão Pebble 5, Vale de Atela Pebble 4, Langford Pebble 1 and Swanscombe Pebble 9 were of relatively lower opacity. The composite structure of Forte do Cão Pebble 2 produce a visible patchwork of relatively transparent and opaque regions.

The natural OSL signal intensity was generally weak, as reflected in the average values of natural OSL: background signal ratio which falls within the range ~1-7 (Table 2, col.2). None of the slices produced a decay curve under IR stimulation, but several slices were found to exhibit IR bleaching, although in these cases there was no consistent evidence of finding markedly lower values of D_e when compared with adjacent slices. A high proportion of the OSL decay curves contained a dominant fast component and the extent of intrusion of a medium component varied both within the same core and between pebbles (examples shown in Supplementary Material, Doc.3, Sec. 1). The OSL trap parameters obtained by performing isothermal decay measurements with one slice from each of seven cores, produced estimates of trapped charge lifetime that were consistent with those reported for the fast component (Timar-Gabor et al., 2017; Durcan, 2018; Singarayer and Bailey, 2004), with values of trap depth between ~1.8 and 2 eV and with the lowest estimates of lifetime at 20 °C exceeding several Ga (Supplementary Material, Doc. 3, Sec. 1).

In one case (Leet Hill, Pebble 4), the OSL decay curves exhibited, in addition to a dominant fast decay component, an elevated 'background' OSL signal which showed only slight reduction under 470 nm stimulation, but could be removed by prolonged UV illumination. Application of the PBG background subtraction procedure was applied to evaluate D_e. (discussed further in Supplementary Material, Doc. 3, Sec. 1). For slices exhibiting satisfactory recycling and dose recovery characteristics, the average values of the recycling ratio (col. 3) and the dose recovery ratio (col. 6) are given for each core in Table 2 (further discussion in Supplementary Material, Doc. 3, Sec. 1). The weighted mean values of the characteristic dose, D_0, for each core are given in col. 4, and the overdispersion (OD, col. 5) observed for most of the cores resulted from the use of a dose range that was optimised for the measurement of D_e rather than a full characterisation of the dose response curve. In the case of 443-2_P2_C1, the average value of D_0 shown is based on 5 slices, but the remaining 12 slices produced significantly higher values of D_0 than the mean value shown and were not included in the calculation due to large uncertainties in D_0 arising from a slightly sub-linear growth within the dose range investigated (~200 Gy). However, the D_0 values calculated are considered sufficient for the purposes of estimating approximate chronological ranges.
The accepted D_e values obtained for slices within each core are discussed in the following section.

5.2 Pebble depth-dose profiles
The D_e values obtained for each slice are plotted against core depth in Figs 3a-e, producing depth-dose (depth-D_e) profiles, and an interpretation of their form and the extraction of average values of D_e is examined in this section. The use of the latter to calculate OSL ages is discussed in Section 5.4 following the assessment of dose rate.

In the case of pebbles tested from the sites of Forte do Cão, Vale de Atela and Langford, sufficient slices were available to obtain depth-D_e profiles using two preheat temperatures (240 and 260 °C). The Leet Hill and Swanscombe depth-D_e profiles are defined predominantly by D_e values that were obtained with a 260 °C preheat, with a few D_e values obtained using the 240 °C preheat to monitor for consistency. The labelled (A or B) horizontal bars in Figs 3a-e indicate the depth range within which an average value of D_e was calculated for the purpose of estimating the OSL age associated with

primary burial (A) and with secondary light exposure and reburial events (B), as discussed in more detail below.

5.2.2 Forte do Cão

Broadly consistent profiles (Fig. 3a(i)) were obtained using two preheat temperatures (240 and 260 °C) with slices from core 4 of Pebble 2 (denoted P2_C4), showing a strong increase in D_e values beyond a depth of ~10 mm. The core extracted from Pebble 2 was drilled from a sloping surface of the wedge-shaped pebble to the opposing flat surface, extending to ~16 mm (P2_C4; Supplementary Material Doc. 2). The plateau in D_e values between the surface and ~8 mm depth (region B; ~1 - ~8 mm) was interpreted to indicate that there had been a stage of in situ secondary light exposure and reburial. The asymmetry in the profile (Fig. 3a(i)) suggests that the pebble had remained stationary during the exposure and that light was predominantly incident on the upper sloping surface (as shown in Supplementary Material Doc. 2), with the other outer surfaces shielded by opaque sediment. The narrow region (A) beyond ~12 mm depth was interpreted to be a remnant of the cumulative (latent) profile developed since primary burial of the sediment. For the purposes of age estimation, average D_e values (Table 3, cols 8,9) of 72.5±5.9 Gy (n=3) and 28.2±0.7 Gy (n=4) were calculated within regions A and B respectively.

The cores extracted from Pebble 5 (P5_C1 and P5_C2), had been drilled orthogonally (Supplementary Material, Doc.2). In the case of C1, the profile (Fig. 3a(ii)) obtained using a 240 °C preheat indicates a systematic rise in D_e values with depth, with a broadly similar trend observed using the higher temperature preheat, albeit with fewer D_e values. The profile for P5_C1 lacks the characteristic steep rise evident in a calculated profile for a lithic clast of effectively semi-infinite dimensions (Fig. 2). A profile of similar slope can be generated using the model, but requires the value of the optical attenuation coefficient, μ, to be reduced by a factor of 10. A visual examination of slices extracted from Pebble 5 indicates, although assessed qualitatively, relatively higher transparency compared with slices from Pebble 2 (Supplementary Material, Fig. SM2.2). The profile obtained with core P5_C2 (Fig. 3a(iii)), was interpreted to contain a narrow plateau within the central region (A), formed by a coherent group (Ward and Wilson, 1978) of D_e values with an average value of 55.5±2.3 Gy (Table 3; 260 °C preheat; T=0.9; $\chi^2_{2,0.05}$=5.99). This value of D_e is consistent with the slightly lower average D_e value obtained with the two deepest slices in C1 (51.0±2.0 Gy; T=2.2; $\chi^2_{1,0.05}$=3.84), where the central axis of the longitudinal core P5_C2 was located at a depth of ~20 mm beneath the first slice of P5_C1 (Supplementary Material, Doc. 2). The average value of D_e within region A of the profile for P5_C2 (55.5±2.3 Gy) was adopted for the calculation of the OSL age of primary burial. In addition, the average of the D_e values obtained for slices flanking region A (42.0±2.1 Gy), located at depths of ~5.5 mm and ~ 16 mm of core P5_C2 (designated B in Fig. 3a(iii)), provide an indicative estimate of the dose accrued since a second stage of exposure and reburial. The measured value of D_e of 72±12 Gy obtained with the sub-surface slice of Pebble 5 (C2, S1), is consistent with the calculated value of 64±11 Gy, which is based on the OSL age estimate for the reburial following a second stage of exposure using the value of D_e defined by B in Fig. 3a(iii) (Supplementary Material, Doc. 3, Sec. 3). If interpreted correctly, this supports the assumption that the inner region (A) of the lower part of Pebble 5 containing core 2 had remained in a dark environment following the second stage of exposure and reburial, dated to ~50 - 70 ka ago, based on the ages calculated using D_e values adopted for region B of the profiles for P2_C4 (47±4 ka) and P5_C2 (71±7 ka), as discussed in section 6.2.

5.2.3 Vale de Atela

The depth-D_e profile obtained with Pebble 4 (P4_C1) is more complex to interpret due to significant differences in the D_e values obtained with 240 and 260 °C preheat temperatures (Fig. 3b(i)) at several depths. In particular, the form of the profile defined by D_e values obtained using the 260 °C preheat appears to be erratic compared with that obtained using the 240 °C preheat. However, the D_e values obtained using the two preheat temperatures that overlap at four depths (shaded boxes) show an

increase with depth similar in general form to that observed with Forte do Cão Pebble 5 (P5_C1, discussed above), but with a steeper gradient overall. For all the D_e values included in the profile, none had failed the SAR acceptance criteria, which included the dose recovery experiments performed using 240 and 260 °C preheats (discussed further below), yet the D_e values (Fig. 3b(i), outlined by box) obtained with quadrants of the deepest slice indicates a systematic difference. The erratic behaviour of the 260 °C PH data does not justify interpreting a plateau in D_e values within the profile, but a value of 98±7 Gy (average of D_e values for slice segments at a depth of 13.9 mm) was extracted for the purposes of calculating an OSL age.

5.2.4 Swanscombe, Barnfield Pit

The profiles obtained for Pebble 2 (Fig. 3c(i)) and Pebble 8 (Fig. 3c(ii)) have broadly similar forms within the interior, each containing an elevated D_e value in the central region that may, as discussed in Section 4, indicate either incomplete resetting or a stage of secondary exposure and reburial. However, the experimental precision in the D_e values is insufficient to confirm that each of the peak values of D_e differ significantly from the values obtained for adjacent slices (P2_C1, T=1.4; $\chi^2_{1,0.05}$=3.84; P8_C1, T=2.4; $\chi^2_{2,0.05}$=5.99). Either side of the centrally located slice in each pebble, the average value of D_e for 6 (P2_C1) and 8 (P8_C1) slices (A, Figs 3c (i) and (ii)) form coherent groups, with weighted average values (Table 3) of 93.6±4.2 Gy (P2_C1; n=6) and 75.8±2.8 Gy (P8_C1; n=8). The significantly lower value of D_e obtained in the outer region (2.35 mm depth) of Pebble 2 suggests optical bleaching of the sub-surface layers. There is clearer indication of effectively uniform secondary light exposure in the profile for Pebble 9 (Fig. 3c(iii)), the profile for which contains a dominant peak and lacks a plateau region within the depth range examined, contrasting with the profiles obtained with pebbles (P2 and P8) from the same context. The peak value of D_e (P, Fig. 3c(iii); D_e= 126±9 Gy) in the profile for Pebble 9 is comparable to those obtained with Pebble 8 (100±12 Gy), and also Pebble 2 (132±22 Gy). Together with the similarity of the pebble mineralogy, this suggests that Pebble 9 was optically reset at deposition to roughly the same extent as for the other pebbles, but the pebble underwent a stage of secondary exposure to light and reburial at a much later stage, sufficient to significantly deplete trapped charge within the outer layers of the pebble. As noted above, Pebble 9 differs from Pebbles 2 and 8 from the same content, its appearance under white light indicating relatively higher transparency (Supplementary Material, Doc. 2, Fig. SM2.2). It is possible that Pebble 9 originated from an overlying deposit that had been disturbed and exposed to sunlight during earlier archaeological work on the site and to have fallen into the sampling area from a backfill deposit during excavation of the sampling pit. Hence, given these uncertainties, an OSL age was not calculated for this pebble.

5.2.5 Leet Hill Quarry

Both depth-D_e profiles obtained with the cores from Pebble 3 (P3_C1; Fig. 3d(i)) and Pebble 4 (P4_C2; Fig. 3d(ii)) indicate the presence of a peak in the central region and a plateau at shallower depths. The peak D_e value (designated A) in the Pebble 3 profile (Fig. 3d(i)) is 85.3±7.9 Gy and the average D_e value within region B is 51.0±2.5 Gy (n=3) if assumed to represent a plateau in D_e values. Similarly, the peak value (designated P) of D_e within the Pebble 4 profile (Fig. 3d(ii)) is 285±62 Gy and the average D_e value obtained within the plateau range A is 111±8 Gy (n=4). This peak value of D_e corresponds to the highest D_e value obtained from all the slices tested, approaching the average value of $2D_0$ for the core (P4_C2). Outwardly, a combination of peak and plateau suggests the occurrence of secondary light exposure and reburial, although, in the case of Pebble 3, this hinges on the D_e value for one slice (~4 mm depth). The two peaks yield significantly different values of D_e, which is not accounted for by differences in the dose rate (Table 3). However, as discussed further below (Section 6.2), reconciliation of the OSL burial age estimates, and agreement with the independent age for the context, can be obtained by arguing for differing interpretations of the optical bleaching histories for these two pebbles from the form of the depth-D_e profiles.

5.2.6 Langford Quarry

The profile obtained for Pebble 1 (Fig. 3e) contains elevated D_e values in the central region (P, $\overline{D}_e$ = 4.9 ± 0.2 Gy) and the surface slice (S1) produced a relatively low value of D_e. Combined, these features are indicative of incomplete depletion of trapped charge prior to the primary burial and a subsequent stage of secondary exposure and reburial. In addition, the measured (2.8 ± 0.5 Gy) value of D_e for the surface slice is significantly lower than the calculated value of 5 ± 1 Gy based on the OSL age estimate for the primary burial (A in Fig. 3e; Table 4), indicating that light exposure affecting the outer layers of the pebble may have occurred. For the purposes of burial age estimation, the D_e values within the depth ranges ~4-6 mm and 12-18 mm (A, Fig. 3e) were interpreted to form plateau regions with a weighted average value of D_e of 3.77 ± 0.25 Gy calculated using the seven D_e values (T=5.8; $\chi^2_{6,0.05}$=12.6) obtained within these depth ranges.

5.3 Dose-rate

The total dose rate calculated for depths greater than 2 mm in cores selected for OSL age evaluation, $\dot{D}_{tot}$, together with a breakdown of the individual components arising from radionuclides within the pebble and the sediment burial medium, and cosmic radiation, listed in Table 3, was calculated using Eqn. 6.

$$\dot{D}_{tot} = a\dot{D}_{\alpha} + \dot{D}_{\beta} + \dot{D}_{\gamma} + \dot{D}_{c} \ , \quad (6)$$

where, a is the alpha efficiency for quartz, $\dot{D}_{\alpha}$ and, $\dot{D}_{\beta}$ are the full energy release alpha and beta dose rates respectively, $\dot{D}_{\gamma}$ is the average gamma dose rate within the pebble volume, adjusted for moisture content of the burial medium, and $\dot{D}_c$ is the cosmic dose rate averaged over the modelled burial history (Supplementary Material, Doc 3, Sec. 3).

The beta and alpha full energy release dose rates were calculated using the conversion factors referred to above and the radionuclide content of the lithics measured by ICP-MS (Supplementary Materials, Table SM3.3). It has been assumed that the very low concentrations of the lithogenic radionuclides in the lithic material measured by ICP-MS in the sub-samples are representative of the pebble interior volume. An average value of 4% was assumed for value of the alpha efficiency, a. This value is similar to that measured by Lai et al. (2008) for quartz extracted from loess, although recent work Bartz et al. (2019), related to the measurements of Al and Ti EPR centres in coarse grain quartz, produced a higher value (7%). While the effect on the total dose rate of such differences in the samples examined in this study is marginal, the efficiency is likely to be sample dependent and would require evaluation if the U/Th content of the pebbles were significantly higher.

The gamma dose rate (Table 3, col. 4), measured at each sampled location was adjusted to account for the effects of moisture content (Aitken, 1985; Nathan and Mauz, 2008). As the moisture content of the interior of the lithic clasts can be assumed to be negligible, the correction was applied only to the contribution to the dose rate arising from the fine fraction of the sediment extracted from each sampled context. The (measured) fraction of the latter by weight within the bulk sample was used to obtain the appropriate weighting factor when calculating the adjusted gamma dose rate. The average burial moisture content applied in this calculation was 24% (the measured average fraction by weight was 22% across the five contexts). The estimated time-averaged values of cosmic dose rate are given in Table 3 (col. 5). Further details of the data used in calculating the dose rate components are provided in the Supplementary Material (Doc. 3, Section 2).

5.4 OSL age estimates

The OSL burial ages, calculated as the quotient of the weighted average value of the equivalent dose, $\overline{D}_e$, and the average total dose rate, $\dot{D}_{tot}$, are listed in Table 3 (A, cols. 6 & 8 ; B, cols. 7 & 9), with an overall uncertainty given at the 68% level of confidence. The latter included an assessment of type A and B standard uncertainties (ISO, 2012) calculated using a procedure based on an analysis of the propagation of experimental errors, similar to that described by Aitken (1985), including the

summing in quadrature of the estimated total uncertainties associated with D_e and the dose rate terms. An uncertainty of ±5% was assigned to type B errors associated with calibrations and the application of conversion coefficients. In addition to type A errors derived from repeated measurements, an uncertainty of ±5% was assigned to type A errors associated with instrument reproducibility in the case of the in situ gamma spectrometry and ±3% in the case of ICP-MS measurements. The OSL ages calculated using values of $\overline{D}_e$ designated 'A', related to the primary burial, are to be compared with the independent age estimates (col. 12). OSL ages calculated using $\overline{D}_e$ values designated 'B', related to a secondary stage of exposure and reburial, are also given for two sites (Forte do Cão, P2 and P5; Leet Hill, P3). In these cases, the estimated OSL ages were calculated using an average cosmic dose rate adjusted for the remaining burial period following the secondary light exposure and reburial, and the infinite medium gamma dose rate was assumed to have been restored relatively promptly.

5.5 Contemporary light exposure

To examine for contemporary optical bleaching affecting the outermost layers, the experimentally determined value of D_e (denoted here as $_mD_e$) obtained with a slice within the sub-surface region (<2 mm depth) was compared with the estimate of D_e (denoted $_cD_e$) derived from the calculated total dose rate ($\dot{D}_{tot}$) for slices cut within this depth range (as discussed above and in Supplementary Material, Doc. 3) and the OSL age estimate for the duration of the last burial stage. The derivation of a value of less than unity for the ratio $_mD_e/_cD_e$ is expected if the outer surface had been optically bleached. The values of these quantities are given in Table 4; the uncertainty associated with the ratio $_mD_e/_cD_e$ in col. 7 is an estimated minimum. In the case of the Swanscombe pebbles, the surface slice S16 was cut from the distal end of pebble P8 and, as the surface slice (S1) of pebble P2 was not suitable for measurement, the D_e value shown is for the second slice (S2).

6. Discussion

6.1 Range

Addressing one of the research questions in this study, the OSL ages obtained for the primary burial of the sampled contexts at the sites of Forte do Cão, Leet Hill and Swanscombe (A, Table 3, col. 10) are in good agreement with the depositional ages assigned on the basis of the independent dating evidence. This agreement is reinforced by the concordance of the results obtained for two pebbles from the same context at these sites. Although the independent dating control for the context sampled at Langford is in the form of a *terminus post quem* (TPQ), the OSL age obtained is consistent with the archaeological evidence from overlying deposits. In contrast, however, the OSL age obtained for the primary burial of the pebbles from Vale de Atela was substantially lower than the independent estimate of age, as discussed further below.

The value of the characteristic dose, D_0, and the dose rate are factors that influence the maximum attainable chronological range, where the limiting value of equivalent dose, D_e, advised in the SAR procedure (Murray and Wintle, 2006) is $2D_0$. Expressed as a proportion of $2D_0$ (Table 2, col. 7), the values of $\overline{D}_e$ associated with the primary burial event ('A' evaluations) ranged from 26% (Swanscombe, 443-2_P2_C1) to 53% (Forte do Cão, 434-1_P2_C4). When the $2D_0$ values are translated to OSL age using their respective total dose rates, the range for the Swanscombe and Leet Hill pebbles is (theoretically) in excess of ~1 Ma. In the case of sedimentary pebbles and their burial environments with low concentrations of radionuclides, as found at these two sites, there is consequently the potential to extend the chronological reach of the technique further, assuming no thermal loss of trapped charge. On the other hand, where the dose rate is higher and a relatively low value of D_0 is obtained, the range is reduced, for example, to ~200 ka in the case of Forte do Cão Pebble 2. The question of whether there are systematic differences between the dose response characteristics of vein quartz and quartzite requires the testing clasts from a much wider selection of sources. At the other end of the chronological range, the possibility of obtaining age estimates with

the much younger late Holocene deposits at Langford flags the potential for working within a wider chronological range than had been initially anticipated.

6.2 Optical resetting and secondary sunlight exposure

The relatively small physical size of pebbles and their consequent mobility would be expected to lead to many episodes of exposure to sunlight during their transport, enabling a higher level of depletion of the legacy trapped charge compared with the interiors of comparatively larger cobbles. The depth-D_e profiles obtained in this study broadly meet this expectation as none contained saturation values of D_e, although the profiles indicate various degrees of optical resetting between the pebbles tested. As discussed above, the presence of a significant peak in the central region of a depth-D_e profile is predicted by the model (History 1) if a residual trapped charge population remained in the central region of a clast before primary burial. In such cases it is not feasible to use the central region of the profile for evaluation of the burial age. However, History 2 illustrates that a central peak may also be present in a profile if a pebble had been uniformly exposed to light at an intermediate stage of the full burial period, followed by reburial. If, in this case, maximal resetting had been obtained before the primary burial, the trapped charge accrued over the full burial period is predicted to be retained, providing the secondary exposure was not long enough to cause a significant loss of trapped charge in the central region before reburial. The self-consistency of OSL age or D_e estimates obtained for primary and potential secondary events is assessed noting this potential ambiguity in the interpretation of a central peak in the profile.

The depth-D_e profiles obtained with the Swanscombe (P2 and P8), Leet Hill (P4) and Langford (P1) pebbles were interpreted to indicate incomplete optical resetting prior to the primary burial, whereas the profiles obtained with the Forte do Cão (P2 and P5), Vale de Atela (P4), Swanscombe (P9) and Leet Hill (P3) pebbles indicated episodes of secondary exposure and reburial.

The least intrusion by a residual peak in the depth-D_e profiles caused by incomplete optical resetting was observed with pebbles (P2 and P8) from the Swanscombe context, where the central region of the profile contained elevated values of D_e values for a single slice. In contrast, the profile obtained with Pebble 4 from Leet Hill (Fig. 3d(ii)), defined by D_e values at three depths of the core (P4_C2: ~9, 12 and 14 mm), presented the strongest intrusions in the measured profiles. A qualitative assessment of transparency indicated that, amongst those tested, this pebble was amongst the most opaque (Supplementary Material, Doc. 2, Fig. SM2.2). Good agreement between the OSL burial age (490±46 ka; Table 3) and the independent age is obtained if the average D_e value for the plateau region (A) in the profile is adopted. This interpretation of the profile assumes that the dominant peak in the profile is due to incomplete resetting prior to primary burial. In the case of Pebble 3 from the same context at Leet Hill, however, concordance of the OSL age with the independent age estimate is obtained if the value of D_e at the peak (A) rather than within region B is adopted for the calculation of the OSL age for the primary burial. The artefacts contained in the Leet Hill Pebble 3 profile are more complex to interpret. On the basis that the OSL age evaluated using the peak value of D_e in the profile is in agreement with the independent age, it could be argued that, similar to History 2 (Fig. 3d(i)), following maximal resetting before primary burial, secondary exposure and reburial occurred at an intermediate stage during the full burial period. The secondary exposure would be required to be sufficient to deplete trapped charge in the outer region of the pebble, but not in the central region. The D_e value obtained for the slice at ~4 mm depth in the profile for Leet Hill Pebble 3 plays a pivotal role in the assessment of whether the D_e values obtained in region B represent a plateau. If the three D_e values form a plateau, an OSL age of 294 ± 28 ka (MIS 8) is obtained by inserting the average value of D_e (B, 51.0 ± 2.5 Gy) in the OSL age equation. However, as the sampled context was overlain by 20 m of deposits and capped by Lowestoft Till associated with Anglian deglaciation, a re-exposure of the sampled context (or penetration of sunlight) ~190 ka following primary burial is unlikely. Sampling within an active quarry, on the other hand, has

attendant risks in terms of disturbance and penetration of sunlight into an exposed face, although a fresh exposure had been created for sampling after the removal of at least 1 m depth of sediment. In the event of contemporary light exposure arising from quarrying activity, the outer layers are, as discussed above, expected to have undergone depletion of trapped charge. Comparison of the measured ($_mD_e$) and calculated ($_cD_e$) values of D_e, obtained with the surface slices of the Leet Hill pebbles (P3 and P4) indicates such a loss ($_mD_e/\ _cD_e$, col. 7, Table 4). In the case of Pebble 3 (P3_C1_S1), this ratio ($_mD_e/\ _cD_e$ = 0.4±0.1) is significantly lower than unity when $_cD_e$ is calculated using the OSL age obtained for the primary burial (A, 490 ka), and a similar value is obtained for Pebble 4 ($_mD_e/\ _cD_e$ = 0.4±0.2). Although the value of this ratio is closer to unity in the case of Pebble 3 based on the age of the putative secondary exposure and burial ($_mD_e/\ _cD_e$= 0.7±0.1(5), Age B), a 'mid-term' secondary exposure is not regarded to be plausible according to the stratigraphic analysis of the section. While the measurements with the sub-surface slices are used here as a test for contemporary light exposure (Sec. 5.5), the extraction of an OSL age for the secondary exposure and reburial would be speculative.

At Swanscombe, the surface slice from the distal part of the P8 core produced a value of D_e that is broadly consistent with the calculated value in the absence of optical bleaching (Table 4, $_mD_e/\ _cD_e$= 1.3±0.3), indicating the absence of secondary light exposure. As suggested above (Section 5.2.4), it is possible that Pebble 9 was intrusive in the sampled context and exposed during earlier fieldwork investigation. In the absence of optical bleaching experiments with whole pebbles to determine the rate of development of the profile under daylight illumination, this interpretation is also speculative. To avoid overinterpretation of a limited set of data, it is important to recall the underlying assumption made in calculating the modelled profiles, that the lithic has a uniform opacity. Localised regions of higher transparency within pebbles would consequently affect the form of the 'depletion' front moving into the lithic under exposure to light, potentially distorting the form of the profile. The extent of such distortion is expected to depend on the complexity of the pathways for the transmission of light within the interiors of quartz and quartzite clasts (Meyer et al., 2018).

Contrary to initial expectation, the size of a residual peak for the late Holocene context at Langford was comparatively small. In this case, subtraction of the average D_e value (3.77 ± 0.25 Gy) calculated within the assigned plateau regions (A; Fig. 3e) from the peak D_e value of ~5 Gy indicates that the dose equivalence of the residual OSL is ~1.2 Gy. However, the degree of resetting can be expected to be sample-specific and likely to be highly variable as the level of maximal resetting is dependent on the duration and intensity of pre-burial optical exposure. Performing the same calculation yields equivalent dose values for the central peak of ~175 Gy in the case of Leet Hill (Pebble 4) and ~20 Gy and ~40 Gy in the case of Pebbles 8 and 2 from Swanscombe, respectively. Nonetheless, these values are orders of magnitude lower than those reported for the inner volumes of larger cobble samples which may be sufficient to saturate the OSL signal. It is also interesting to note the higher OSL sensitivity found with the pebble from Langford produced natural OSL signals that were comparable with those obtained with pebbles from the considerably older contexts of the other sites. The higher concentration of large pebbles at Langford suggests a shorter period of transport when compared with the relatively sparse quantity of pebbles from the older sites. This would be contrary to expectation for fluvial sediments where it has been argued (Pietsch et al., 2008) that the OSL sensitivity of sedimentary quartz increases with the extent of transport and weathering, although, as pointed out by Sawakuchi et al. (2011), the underlying variability in the luminescence sensitivity of hydrothermal vein quartz is primarily attributed to differences in crystallization temperature.

The strongest signature of a secondary stage of light exposure and reburial in the depth-D_e profiles, was obtained with the Forte do Cão Pebble 2, which raises the issue of depletion of the trapped charge accumulated since burial, leading to underestimation of the full burial period. The OSL age

obtained for the primary burial of Pebble 2 (434-1_P2_C4; 115±13 ka) is in good agreement with the independent age control, indicating the absence of a significant effect on trapped charge in the deeper section of the core (range A, Fig. 3a(i)). On the other hand, the OSL age for the primary burial of Pebble 5 (434-1_P5_C2; 89±8 ka), while overlapping with the age interval for MIS 5 assigned to its context, differs from the OSL age for Pebble 2 when tested statistically on the basis of Type A errors ($T=5.4$; $\chi^2_{1,0.05}=3.84$). Hence there is the possibility that the depth range within Pebble 5 used for age evaluation (A, Fig. 3a(iii)) may have suffered some charge depletion during the indicated secondary exposure before reburial, made more likely by the higher transparency indicated for this pebble (Supplementary Material, Doc. 2, Fig. SM2.2), as reflected in the form of the profile obtained for its companion, Core 1. The OSL age calculated for the reburial of Pebble 2 following a stage of secondary exposure, 47±4 ka (B, Table 1), places the event within the range of MIS 3. An estimate of the age of this event can also be obtained from Pebble 5 (core 2), the OSL age estimate for which is older (71±7 ka) but, as discussed above (Sec. 5.2.2), this is a necessarily tentative estimate in the absence of a defined plateau and being based on the results for only two slices. More speculatively, the lack of significant aggradation of sediment at this site for an estimated period of ~70 ka (Supplementary Material, Doc. 3, Fig. SM3.6, Forte do Cão), indicated by a stratigraphic analysis of the terrace sequence, raises the possibility of an erosive event sufficient to enable the penetration of sunlight into the sampled context. Returning to the model, if secondary exposure period is constrained to 70 ka, a profile with a depth of penetration similar to the measured profile (as in History 3, Fig. 2c) is obtained by selecting a value for $\overline{\sigma\Phi_0}$ that is about three times the primary value used (6.34×10^{-9} s^{-1}).

Over and above the difficulties in interpreting the depth-D_e profile obtained with the Vale de Atela pebble (Sec. 5.2.3), the OSL age (176±18 ka) calculated using a D_e value in the upper range of values obtained with slices in the central region represents a substantial underestimate of the independent age assigned to the context (MIS 9). Although the profile for Vale de Atela Pebble 4 (Fig. 3b(i)) similar in form to the profile obtained with Forte do Cão Pebble 5 (Fig. 3a(ii)), the shortfall in age indicates that significant charge depletion extended to the deeper parts of the pebble at a post-depositional stage. The generation of such a profile could be accounted for by a complete optical resetting at ~180 ka ago, followed by an in situ secondary light exposure at a later stage, where trapped charge in the deeper layers remained intact. However, given the erratic reproducibility of the D_e values, pebbles with better luminescence characteristics are required to investigate this issue further. It is worth noting that where sampling is performed on escarpments (such as at Vale de Atela, Leet Hill and Langford), sampling to much greater depth may be advisable to reduce the risk of the penetration of scattered sunlight into exposures following natural erosion or quarrying processes.

6.3 Dose rates

The values of total dose rate, ranging from ~170- 630 mGy ka^{-1}, are very low compared with those expected for granular quartz inclusions in typical sediment deposits, for example. With two exceptions, the major contributors to the dose rate (Table 3) are the external gamma and cosmic components of the dose rate, which range as a proportion of the total dose rate, $\dot{D}_{tot}$, from 52% (443-2, P2) to 92% (435-2, P1) for the gamma component and 17% (441-2_P4) to 35% (443-2_P8) for the cosmic component. The internal pebble dose rate (α and β radiation) contributes less than 5% of the total, except in the case of pebbles from Leet Hill (441-2_P4) and Swanscombe (443-2_P2) where it is much larger (25% and 20% respectively). When calculating the dose rate due to sources within the pebble, on the basis of the analytically determined radionuclide concentrations, it was assumed that they were uniformly distributed within the lithic. If that were not the case, there is the potential for fluctuations to be introduced to the form of the depth-D_e profile in cases where the concentrations were significantly higher. While the volume of the slices used to evaluate D_e is likely to dampen such effects, the assessment of dose-rate in these circumstances would be problematic,

as encountered in previous studies (e.g., Tribolo et al., 2013). Hence an assessment of bulk radioactive content of the lithics at an early stage is advisable to enable the proportion of the total dose contributed by sources within the lithic to be assessed.

In the case of Leet Hill and Swanscombe, consistent ages were obtained for each depositional context where the two pebbles tested had different internal dose rates $\dot{D}_{tot}$ (441-2, P3 vs P4 and 443-2, P2 vs P8). Although in these particular circumstances independent age controls were available, the testing of pebbles from the same context with differing internal dose rates provides the opportunity to test for age concordance and the self- consistency of the assessment of dose rate.

6.4 Application

The results of this study indicate that clasts of pebble dimensions, in the form of vein quartz or quartzite, are likely to have had a substantial part of their volume sufficiently optically reset by exposure to sunlight during their history of transport and mobilisation. This provides the opportunity for application in both environmental and archaeological contexts where these mineral clasts are present, potentially over a very wide chronological range. Previous OSL dating studies (e.g., Pawley et al.,2008) based on coarse grain quartz measurements, have successfully exploited the opportunity available within relatively weakly radioactive sedimentary environments to significantly extend the chronological reach of OSL beyond its typical range. Further reduction in the total dose rate by the use of the interior parts of pebbles enables the potential of yet further extension of the working range to be realised. This capability has been demonstrated with independently dated contexts to ~500 ka and the testing of progressively older deposits with dating control is required to explore whether the combination of experimental techniques and the various assumptions discussed above produce reliable determinations of age within the upper technical limit of the method, as governed by D_e saturation and the total dose rate. While we have selected sites with terrace deposits representing two types of depositional environment (fluvial and coastal marine) there are others where the sampling of small lithic clasts such as pebbles could provide date estimates that have not been possible using other methods.

In principle, higher opacity enables, after a sufficient burial period, an optical exposure event following primary burial to be detected by modification of the depth-dose profile. Such modification is in addition to any inherited profile resulting from incomplete optical resetting before the primary burial. Clasts possessing higher transparency have the advantage of undergoing more rapid optical bleaching prior to burial, aided by internal scattering of light within the clast once transmitted through any outer weathering skin. However, as a consequence, the depth-dose profiles measured within them provide a less pronounced signature of any subsequent light exposure events, lacking the distinctive stepped profile predicted for lithics of higher opacity (Freiesleben et al., 2015). In the case of the excavation of archaeological sites where the overburden is substantial (e.g., > 1m) and undisturbed, the exposure of a context of interest can be controlled and the risk of substantial resetting reduced. On the other hand, the experience of sampling quarry and natural exposures in this study (e.g., Vale de Atela), the effects of penetrating scattered sunlight may require more cautious preparation for sampling and retrieval at much greater depth (i.e., >1m). If present within the same context, the testing of pebbles with differing transparency would enable assumptions regarding primary and secondary light exposure within a buried context formed by naturally or anthropogenically controlled depositional processes to be tested.

On the basis of the characteristics of pebbles from the Late Pleistocene sites examined in this study, the OSL signal strength would not be expected to be sufficient to determine a burial period within the Holocene. However, the results obtained with the Langford pebble indicate the potential value of further investigation of dating Holocene depositional processes with quartzose lithics. Although this represents only one example, the luminescence characteristics, in particular OSL sensitivity, of

quartz or quartzite pebbles are known to vary widely according to the source of the original lithic clasts. The portability of smaller lithic clasts has a particular relevance to anthropogenic processes. Where pebbles have been collected from surficial contexts in fluvial or coastal beach environments, for use in tool manufacture or for other purposes (Tilley et al., 2017), optical resetting associated with the process of deposition or discard within a site may not be critical if the pebbles were sufficiently reset within the catchment area. In the case of standing stone monuments, for example, it is frequently difficult to find suitable organic samples for radiocarbon dating that can be securely linked to the original construction of the monument. Where quartz or quartzite pebbles and cobbles were used as packing stones in the sockets (e.g., Bradley, 2016), there is the potential to date the construction of the monument by the combined application of OSL to both the lithic clasts and the finer sediment forming their burial medium. There are also contexts associated with the dating of rock shelter sites where this approach applied to unheated quartz pebbles could be productive (e.g., Asfora et al., 2014).

7. Conclusion

By virtue of their size and sedimentary history (e.g., transport), quartzose pebbles within fluvial and coastal beach deposits, or those of similar origin subsequently introduced into sedimentary contexts by anthropogenic processes, have the potential to serve as chronological markers for a range of depositional processes. Although this is an exploratory study with a limited number of pebbles tested, the results indicate that the application of SAR OSL measurement procedures to vein-quartz and quartzite pebbles from fluvial and coastal beach contexts has the potential to date burial processes across a broad chronological range, from the late Holocene to ~500 ka. The initial expectation that a substantial extension of the typical OSL range for granular quartz, could be obtained by a significantly reduced dose rate was confirmed, arising from a combination of very low concentrations of lithogenic radionuclides within the pebbles and also moderate to low concentrations of these sources within the sediment forming the local burial medium. The relatively low concentrations of radionuclides within the quartzose pebbles also simplifies the assessment of the dose rate. Furthermore, there was evidence within some of the pebbles of the capacity to further extend the range as the age equivalence of the limiting value of D_e is in excess of 1 Ma, thermal stability of trapped charge permitting. However, the combination of poor luminescence characteristics and uncertain secondary light exposure history may give rise to difficulties in extracting reliable age estimates, as encountered with the pebble from the Vale de Atela context, and the testing of a wider range of source material is required to optimise sample selection. As has been noted in previous studies with cobbles, the approach relies on the measurement and interpretation of depth-dose profiles to identify key stages in the burial history including the extent of pre-burial optical resetting, primary burial and subsequent secondary light exposure and reburial. Continued testing with lithics from contexts having depositional histories with independent age control, where available, will be important to test these interpretations. While some of the pebbles had not been fully reset before burial, none were in field saturation, as commonly encountered with larger lithic clasts such as cobbles. The advantages of working with smaller clast in the form of pebbles and with a lithology of higher transparency opens up a wide range of potential applications, whether the depositional processes are natural or anthropogenic in origin or modification.

Acknowledgements

This research was supported by Durham University (IKB and DB), and the contribution of Pedro P. Cunha was funded by the Fundação para a Ciência e Tecnologia (FCT), through: (i) national funds, by the projects UIDB/MAR/04292/2020 — MARE (Marine and Environmental Sciences Centre); (ii) a Sabbatical grant, with ref. SFRH/BSAB/150395/2019 (Programa Operacional Capital Humano).
For permission to obtain samples we thank: Tarmac plc (Langford Quarry) and Tom Keyworth, Trent and Peak Archaeology for facilitating access; LP Pallet Esq (Leet Hill Quarry); the General Manager of Pontins Pakefield; the leaders of the INQUA field excursion *Quaternary Fluvial Archives of the Major*

English Rivers, including Beccy Briant, Peter Allen, Eleanor Brown and Tom White, for facilitating sampling at Swanscombe; to Eleanor Brown, English Nature, Mark White and Dave Roberts, Durham University and Rob Westaway, University of Glasgow, for advice on accessing sites; to Ricardo Carvalhido and Antonio Martins for their help with sampling and lithostratigraphic assessment of, respectively, the Forte Cão and Vale de Atela sites. We also thank Eric Andrieux for assistance in producing the sedimentary log illustrations, Alejandra Gutiérrez for advice on maps and Lily Bossin and Stephen Barnard for performing an irradiation of core slices at the Medical Research Council ^{60}Co Irradiation Facility, Harwell Campus, Didcot, UK, where access was enabled by Public Health England. We thank the reviewers for their detailed and constructive comments on the submitted manuscript.

References

Aitken, M.J., 1985. Thermoluminescence Dating. Academic Press, London.

Asfora, V., Guzzo, P., Pessis, A., Barros, V., Watanabe, S., Khoury, H., 2014. Characterization of the burning conditions of archaeological pebbles using the thermal sensitization of the 110 °C TL peak of quartz. Radiation Measurements 71, 485-489. https://doi.org/10.1016/j.radmeas.2014.04.022

Bailiff, I.K., 2018. An examination of beta dose attenuation effects in coarse grains located in sliced samples. Radiation Measurements 120, 188-194. https://doi.org/10.1016/j.radmeas.2018.07.015

Bailiff, I.K., French, C.A., Scarre, C.J., 2014. Application of luminescence dating and geomorphological analysis to the study of landscape evolution, settlement and climate change on the Channel Island of Herm. Journal of Archaeological Science 41, 890-903. https://doi.org/10.1016/j.jas.2013.10.014

Bartz, M., Arnold, L.J., Spooner, N.A. et al. First experimental evaluation of the alpha efficiency in coarse-grained quartz for ESR dating purposes: implications for dose rate evaluation. Sci Rep 9, 19769 (2019). https://doi.org/10.1038/s41598-019-54688-9

Bateman, M.D. (2019) Handbook of Luminescence Dating (ed., M.D. Bateman). Whittles Publishing, Caithness, Scotland.

Bradley, R. 2016. Croftmoraig: the anatomy of a stone circle. *In The Use and Reuse of Stone Circles: Fieldwork at Five Scottish Monuments and its Implications* (Eds R. Bradley and C. NImura). Oxbow Books, Oxford, UK.

Bridgland, D.R., 1994. Quaternary of the Thames. Geological Conservation Review Series, 7, Chapman & Hall, London.

Bridgland, D.R., Howard, A.J., White, M.J., White, T.S. (Eds), 2014. Quaternary of the Trent. Oxbow Books, Oxford. ISBN 978-1-78297-024-8

Bridgland, D.R., Briant, R.M., Allen, P., Brown, E.J., White, T.S., 2019. The Quaternary fluvial archives of the major English rivers: Field Guide. Quaternary Research Association, London.

Carvalhido, R.P., Pereira, D.I., Cunha, P., Buylaert, J.P., Murray, A.S. 2014. Characterization and dating of coastal deposits of NW Portugal (Minho–Neiva area): A record of climate, eustasy and crustal uplift during the Quaternary. Geology 328-329, 94-106. https://doi.org/10.1016/j.quaint.2014.01.025

Cunha, P.P., Martins, A.A., Buylaert, J.P., Murray, A.S., Raposo, L., Mozzi, P., Stokes, M., 2017. New data on the chronology of the Vale do Forno sedimentary sequence (Lower Tejo River terrace staircase) and its relevance as a fluvial archive of the Middle Pleistocene in western Iberia, Quaternary Science Reviews 166, 204-226. https://doi.org/10.1016/j.quascirev.2016.11.001

Duller, G. A. T., 2003. Distinguishing quartz and feldspar in single grain luminescence measurements, Radiation Measurements 37, 161–165. https://doi.org/10.1016/S1350-4487(02)00170-1

Durcan, J. A., 2018. Assessing the reproducibility of quartz OSL lifetime determinations derived using isothermal decay. Radiation Measurements 120, 234-240. https://doi.org/10.1016/j.radmeas.2018.06.020

Erlykin, A.D., Wolfendale, A.W., Long term time variability of cosmic rays and possible relevance to the development of life on Earth. Surveys in Geophysics 31:383–398. https://doi.org/10.1007/s10712-010-9097-8

Freiesleben, T., Sohbati, R., Murray, A., Jain, M., Al Khasawneh, S., Hvidt, S., Jakobsen, B., 2015. Mathematical model quantifies multiple daylight exposure and burial events for rock surfaces using luminescence dating. Radiation Measurements 81, 16- 22. https://doi.org/10.1016/j.radmeas.2015.02.004

Gliganic, L.A., Meyer, M.C., Sohbati, R., Barrett, S., 2019, OSL surface exposure dating of a lithic quarry in Tibet: laboratory validation and application. Quaternary Geochronology, 49, 199–204.

(http://laws.lanl.gov/vhosts/mcnp.lanl.gov/pdf_files/la-ur-13-22934.pdf

Guralnik, B., Ankjærgaard, C., Jain, M., Murray, A.S., Müller, A., Wälle, M., Lowick, S.E., Preusser, F., Rhodes, E.J., Wu, T.S., Mathew, G., Herman, F., 2015. OSL-thermochronometry using bedrock

quartz: A note of caution. Quaternary Geochronology 25, 37-48. https://doi.org/10.1016/j.quageo.2014.09.001
Guérin, G., Mercier, N., Adamiec, G., 2011. Dose-rate conversion factors: update, Ancient TL 29, 5-8.
Howard, A.J., Smith, D.N., Garton, D., Hillam, J., Pearce, M., 2000. Middle to Late Holocene environments in the Middle to Lower Trent Valley. In *Fluvial Processes and Environmental Change* (eds. A.G. Brown and T.A. Quine) Wiley, Chichester, 165-178.
Howard, A.J., 2005. The contribution of geoarchaeology to understanding the environmental history and archaeological resources of the Trent Valley, U.K. Geoarchaeology 20, 93-107. https://doi.org/10.1002/gea.20038
Huntley, D. J., Richards, M., 1997. The age of the Diring Quriakh archaeological site. Ancient TL 15, 48–51.
ISO, 2012, International vocabulary of metrology - Basic and general concepts and associated terms (VIM). 3rd Edition. JCGM 200:2012. http://www.bipm.org/vim
Jenkins, G.T.H., Duller, G.A.T., Roberts, H.M., Chiverrell, R.C., Glasser, N.F., 2018 A new approach for luminescence dating glaciofluvial deposits – High precision optical dating of cobbles. Quaternary Science Reviews 192, 263-273. https://doi.org/10.1016/j.quascirev.2018.05.036
King, G.E., Valla, P.G., Lehmann, B., 2019. Rock surface burial and exposure dating. In *Handbook of Luminescence Dating* (Ed M. D. Bateman). Whittles Publishing, Caithness, Scotland, UK.
Lai, Z.P., Zöller, L., Fuchs, M., Brückner, H., 2008. Alpha efficiency determination for OSL of quartz extracted from Chinese loess. - Radiation Measurements 43, 767-770. https://doi.org/10.1016/j.radmeas.2008.01.022
Laskaris, N., Liritzis, I., 2011. A new mathematical approximation of sunlight attenuation in rocks for surface luminescence dating. J. Luminescence 131, 1874-1884. https://doi.org/10.1016/j.jlumin.2011.04.052
Meyer, M.C., Gliganic, L.A., Jain, M., Sohbati, R., Schmidmair, D., 2018. Lithological controls on light penetration into rock surfaces – Implications for OSL and IRSL surface exposure dating. Radiation Measurements 120, 296-304. https://doi.org/10.1016/j.radmeas.2018.03.004
Mozzi, P., Azevedo, M.T., Nunes, E., Raposo, L., 2000. Middle terrace deposits of the Tagus River in Alpiarça, Portugal, in relation to early human occupation. Quaternary Research 54, 359-371. 10.1006/qres.2000.2154
Munyikwa, K., 2000. Cosmic ray contribution to environmental dose rates with varying overburden thickness. Ancient TL 18, 27-18.
Murray, A.S., Wintle, A.G., 2000, Luminescence dating of quartz using an improved single-aliquot regenerative-dose protocol. Radiation Measurements 32, 57–73. https://doi.org/10.1016/S1350-4487(99)00253-X
Murray, A.S., Wintle, A.G., 2003, The single aliquot regenerative dose protocol: potential for improvements in reliability. Radiation Measurements 37, 377–381. https://doi.org/10.1016/S1350-4487(03)00053-2
Nathan, R.P., Mauz, B., 2008. On the dose-rate estimate of carbonate-rich sediments for trapped charge dating. Radiation Measurements 43, 14-25. https://doi.org/10.1016/j.radmeas.2007.12.012
Ou, X.J., Roberts, H.M., Duller, G.A.T., Gunn, M.D., Perkins, W.T., 2018. Attenuation of light in different rock types and implications for rock surface luminescence dating. Radiation Measurements 120, 305-311. https://doi.org/10.1016/j.radmeas.2018.06.027
Pawley, S.M., Bailey, R.M., Rose, J., Moorlock, B.S.P., Hamblin, R.J.O., Booth, S.J., Lee, J.R., 2008. Age limits on Middle Pleistocene glacial sediments from OSL dating, north Norfolk, UK. Quat.Sci.Rev. 27, 1363–1377. https://doi.org/10.1016/j.quascirev.2008.02.013
Pietsch, T.J., Olley, J.M., Nanson, G.C., 2008. Fluvial transport as a natural luminescence sensitiser of quartz. Quaternary Geochronology 3, 365–376. https://doi.org/10.1016/j.quageo.2007.12.005
Polikreti, K., Michael, C.T., Maniatis, Y., 2002. Authenticating marble sculpture with thermoluminescence. Ancient TL 20, 11-18.

Preece, R. C., Parfitt, S. A., Coope, G. R., Penkman, K. E. H., Ponel, P., Whittaker, J. E., 2009. Biostratigraphic and aminostratigraphic constraints on the age of the Middle Pleistocene glacial succession in north Norfolk, UK. J. Quaternary Sci. 24 557–580. https://doi.org/10.1002/jqs.1245

Prescott, J.R., Hutton, J.T., 1988. Cosmic ray and gamma ray dosimetry for TL and ESR. Radiation Measurements 14, 223-227. https://doi.org/10.1016/1359-0189(88)90069-6

Prescott J.R., Hutton J.T., 1994. Cosmic ray contribution to dose rates for luminescence and ESR dating: large depths and long-term time variations. Radiation Measurements 23, 497-500. https://doi.org/10.1016/1350-4487(94)90086-8

Rades, E.F., Sohbati, R., Lüthgens, C., Jain, M., Murray, A.S., 2018. First luminescence-depth profiles from boulders from moraine deposits: Insights into glaciation chronology and transport dynamics in Malta valley, Austria. Radiation Measurements 120, 281-289. https://doi.org/10.1016/j.radmeas.2018.08.011

Riedesel, S., Autzen, M., 2020. Beta and gamma dose rate attenuation in rocks and sediment. Radiation Measurements 133, 106295. https://doi.org/10.1016/j.radmeas.2020.106295

Roberts, H.M., Duller, G.A.T., 2004. Standardised growth curves for optical dating of sediment using multiple-grain aliquots. Radiation Measurements 38, 241-252. https://doi.org/10.1016/j.radmeas.2003.10.001

Rose, J., Lee, J.A., Candy, I., Lewis, S.G., 1999. Early and Middle Pleistocene river systems in eastern England: evidence from Leet Hill. J Quaternary Science 14, 347-360. https://doi.org/10.1002/(SICI)1099-1417(199907)14:4%3C347::AID-JQS456%3E3.0.CO;2-A

Singarayer, J.S., Bailey, R.M., 2004. Component- resolved bleaching spectra of quartz optically stimulated luminescence: preliminary results and implications for dating. Radiation Measurements 38, 111–118. https://doi.org/10.1016/S1350-4487(03)00250-6

Sawakuchi, A.O., Blair, M.W., DeWitt R., Faleiros, F.M., Hyppolito, T., Guedes, C.C.E., 2011. Thermal history versus sedimentary history: OSL sensitivity of quartz grains extracted from rocks and sediments. Quaternary Geochronology 6, 261-272. https://doi.org/10.1016/j.quageo.2010.11.002

Simkins, L.M., DeWitt, R., Simms, A.R., Briggs, S., Shapiro, R.S., 2016. Investigation of optically stimulated luminescence behavior of quartz from crystalline rock surfaces: A look forward. Quaternary Geochronology 36, 161-173. https://doi.org/10.1016/j.quageo.2016.09.002

Simms, A.R., DeWitt, R., Kouremenos, P., Drewry, A.M., 2011. A new approach to reconstructing sea levels in Antarctica using optically stimulated luminescence of cobble surfaces. Quaternary Geochronology 6, 50-60. https://doi.org/10.1016/j.quageo.2010.06.004

Sohbati, R., Murray, A., Jain, M., Buylaert, J.-P., Thomsen, K., 2011. Investigating the resetting of OSL signals in rock surfaces. Geochronometria 38, 249-258. https://doi.org/10.2478/s13386-011-0029-2

Sohbati, R., Murray, A., Chapot, M.S., Jain, M., Pederson, J., 2012a. Optically stimulated luminescence (OSL) as a chronometer for surface exposure dating. J Geophysical Research 117, B09202. https://doi.org/10.1029/2012JB009383

Sohbati, R, Murray, AS, Buylaert, J-P, Almeida, N., Cunha, P., 2012b. Optically stimulated luminescence (OSL) dating of quartzite cobbles from the Tapada do Montinho archaeological site (east-central Portugal), Boreas 41, 452-462. https://doi.org/10.1111/j.1502-3885.2012.00249.x

Sohbati, R., Jain, M., Murray, A., 2012c. Surface exposure dating of non-terrestrial bodies using optically stimulated luminescence: A new method. Icarus 221, 160-165. https://doi.org/10.1016/j.icarus.2012.07.017

Souza, P.E., Sohbati, R., Murray, A.S., Kroon, A., Clemmensen, L.B., Hede, M.U., Nielsen, L., 2019. Luminescence dating of buried cobble surfaces from sandy beach ridges: a case study from Denmark. Boreas. https://doi.org/10.1111/bor.12402

Tilley, C., Allen, M.J., Cobley, J., Merion Jones, A., Pauknerova, K., Sanfelice Rahmeier, C., Trenchard, P., 2017. Landscape in the Longue Durée: A History and Theory of Pebbles in a Pebbled Heathland Landscape. UCL Press, London, UK. https://doi.org/10.2307/j.ctt1vxm8qq

Timar-Gabor, A., Buylaert, J. -P., Guralnik, B., Trandafir-Antohi, O., Constantin, D., Anechitei-Deacu, V., Jain, M., Murray, A. S., Porat, N., Hao, Q., Wintle, A. G., 2017. On the importance of grain size in luminescence dating using quartz. Radiation Measurements 106, 464-471. https://doi.org/10.1016/j.radmeas.2017.01.009

Tribolo, C., Mercier, N., Douville, E., Joron, J.-L., Reyss, J.-L., Rufer, D., Cantin, N., Lefrais, Y., Miller, C.E., Parkington, J., Porraz, G., Rigaud, J.-P., Texier, P.-J., 2013. OSL and TL dating of the middle stone age sequence of Diepkloof rock shelter (Western Cape, South Africa): a clarification. J. Archaeological Science 40, 3401–3411. https://doi.org/10.1016/j.jas.2012.12.001

Vafiadou, A., Murray, A.S., Liritzis, I., 2007. Optically stimulated luminescence (OSL) dating investigations of rock and underlying soil from three case studies. Journal of Archaeological Science 34, 1659-1669. https://doi.org/10.1016/j.jas.2006.12.004

Ward, G.K., Wilson, S.R., 1978. Procedures for comparing and combining radiocarbon age determinations: a critique. Archaeometry 20, 19-31. https://doi.org/10.1111/j.1475-4754.1978.tb00208.x

Westaway, R., 2009. Quaternary vertical crustal motion and drainage evolution in East Anglia and adjoining parts of southern England: chronology of the Ingham River terrace deposits. Boreas 38, 261–284. https://doi.org/10.1111/j.1502-3885.2008.00068.x

White, T.S., Preece, R.C., Whittaker, J.E., 2013. Molluscan and ostracod successions from Dierden's Pit, Swanscombe: insights into the fluvial history, sea-level record and human occupation of the Hoxnian Thames. Quaternary Science Reviews 70, 73–90. https://doi.org/10.1016/j.quascirev.2013.03.007

Wintle, A.G., Murray, A.S., 2006, A review of quartz optically stimulated luminescence characteristics and their relevance in single aliquot regeneration dating protocols. Radiation Measurements 41, 369–391. https://doi.org/10.1016/j.radmeas.2005.11.001

Table 1. Model parameters

a) Optical

	Stages	Units	History 1	History 2	History 3
$\overline{\sigma\Phi_0}$ = 6.34 x 10^{-9} s^{-1} μ = 1 mm^{-1}	1. Exposure	ka	10	500	500
	2. Burial	ka	500	180	280
	3. Exposure	a	2	$2x10^3$	$3x10^5$
	4. Burial	ka	-	320	220
	5. Exposure	a		2	2
$\overline{\sigma\Phi_0}$ = 6.34 x 10^{-6} s^{-1} μ = 1 mm^{-1}	1. Exposure	a	3	250	250
	3. Exposure	a	$2x10^{-3}$	2	300
	5. Exposure	d	-	0.75	$2x10^{-3}$

b) Dose response and dose rate

D_0	b_l	b_s	$_{lith}\dot{D}_\beta^\infty$	$_{sed}\dot{D}_\beta^\infty$	$_{sed}\dot{D}_\gamma + \dot{D}_{cos}$
Gy	mm^{-1}	mm^{-1}	Gy ka^{-1}	Gy ka^{-1}	Gy ka^{-1}
120	2.0	3.1	0.05	0.60	0.20

Notes

In Table 1b, the values of D_0 and the infinite medium beta and gamma dose rates were selected to broadly reflect the values measured with materials from the study sites. The beta attenuation factors, b_l (lithic) and b_s (sediment) represent weighted mean values calculated for the radionuclide composition adopted for the model illustration, as discussed in the main text.

Table 2. OSL parameters

Sample	Signal : PBG (RSD%)	Recycling Ratio	$\overline{D_0}$	OD	DRec $\frac{\overline{D_e}}{D_a}$	$\frac{\overline{D}_e}{2\overline{D}_0}$
			(Gy)	%		%
Col.# (1)	(2)	(3)	(4)	(5)	(6)	(7)
Forte Cão						
434-1_P2_C4	2.5 (12%)	0.95±0.20 (14)	68±4 (11)	15	0.93±0.25 (4)	53
_P5_C1	3.3 (21%)	0.92±0.05 (9)	94±8 (8)	17	1.05±0.10 (4)	
_C2	2.9 (5%)	1.02±0.09 (11)	82±6 (10)	4	1.08±0.10 (6)	34
Vale de Atela						
434-2_P4_C1	6.7 (51%)	0.99±0.10 (19)	130±7 (19)	14	0.98±0.11 (7)	38
Langford						
435-2_P1_C1	1.8 (22%)	0.94±0.05 (9)	-		1.04±0.17 (6)	-
Leet Hill						
441-2_P3_C1	3.0 (30%)	0.91±0.11 (10)	157±19 (8)	31	0.94±0.16 (4)	27
P4_C2	0.9 (27%)	0.98±0.18 (10)	143±15 (5)	13	0.95±0.08 (2)	39
Swanscombe						
443-2_P2_C1	2.7 (41%)	0.96±0.17 (6)	181±12 (5)	0	1.07±0.15 (2)	26
_P8_C1	5.6 (36%)	0.93±0.12 (9)	107±7 (11)	15	1.05±0.20 (1)	35
-P9_C1	3.0 (33%)	0.86±0.09 (5)	126±11 (7)	17	1.08±0.20 (2)	-

Notes

1. The Signal:PBG corresponds to the ratio of the natural (I_N) and background (I_{BG}) OSL signals as measured in the SAR procedure (Steps 1 and 2; Supplementary Material, Table SM3.1). The RSD was calculated for those slices producing accepted values of D_e.
2. The recycling ratio (col. 3) corresponds to the ratio of sensitivity-corrected values, $I_{\beta 8}/I_{\beta 2}$ in the SAR procedure (Supplementary Material, Table SM3.1).
3. The values in col. 6 correspond to the ratio of the evaluated dose D_e and the applied dose, D_a, obtained in the dose recovery (DRec) experiment.
4. The values of the recycling ratio (col. 3) and D_e/D_a (col. 4) are given as mean values for the slices producing accepted value of D_e in the core indicated, together with their standard deviations (n>1), where the number of determinations, n, is given in parentheses.
5 The values of the dose characteristics, D_0, in col.5 are weighted mean values calculated for slices producing accepted values of D_e. They are given with the standard error, the number of determinations in parentheses (col. 4), and the overdispersion (col. 5).
6. The value of $\overline{D}_e$ used to calculate the value shown in col. 7 corresponds to the weighted average value shown in col. 12 of Table 1 in the main text.

Table 3. OSL age calculation data

Sample	Dose rate						Equivalent Dose		OSL Age	OSL Age	Independent
	a$\dot{D}_{\alpha}$	$\dot{D}_{\beta}$	$\dot{D}_{\gamma}$	$\dot{D}_{c}$	$\dot{D}_{tot}$ A	$\dot{D}_{tot}$ B	$\bar{D}_{e}$ A	$\bar{D}_{e}$ B	A	B	Age
	(mGy ka^{-1})						(Gy)	(Gy)	(ka)	(ka)	(ka)
Col.# (1)	(2)	(3)	(4)	(5)	(6)	(7)	(8)	(9)	(10)	(11)	(12)
Forte do Cão											
434-1_P2_C4	7	6	465	154	632±23	603±23	72.5±5.9	28.2±0.7	115±13	47±4	115-105
_P5 _C1	1.4	1.6	465	154	622±23		51.0±2.0		82±8		(MIS 5)
_C2						593±23	55.5±2.3	42.0±2.1	89±8	71±7	
Vale de Atela											
434-2_P4_C1	14	19	427	96	556±21		98.0±7.0		176±18		320-300 (MIS 9)
Langford											
435-2_P1_C1	6	7	343	130	486±34		3.77±0.25		7.8±0.9		Late Holocene
Leet Hill											
441-2_P3_C1	3	3	130	37	173±7	173±7	85.3±7.9	51.0±2.5	492±61	294±28	MIS 12
P4_C2	10	49	130	37	226±7		111.0±8.0		490±46		(478-424)
Swanscombe											
443-2_P2_C1	14	34	128	70	246±7		93.6±4.2		380±29		MIS 11c
_P8_C1	2	2	128	70	202±13		75.8±2.8		375±37		(420-390)

Notes.

1. The components of dose rate (cols 2-7), the derivation of average values of D_e (cols 8 and 9) and the calculation of OSL age (cols 10 and 11) are discussed in sections 5.3, 5.2 and 5.4, respectively, of the main text.
2 The OSL age test year was CE 2019. Uncertainties are given at the 68% level of confidence (1σ); those associated with the OSL age represent the overall error that includes type A and B errors combined in quadrature. The components of the total dose rate are given (cols 2-5) as central values; the estimates of their type A uncertainties are incorporated in the (type A) uncertainty given with the total dose rate (cols. 6, 7), as discussed in the main text.
2. Independent age ranges for the sampled context assigned primarily either within the indicated marine isotope stage (MIS) or approximate absolute chronological range, as discussed in the main text.

a)

b)

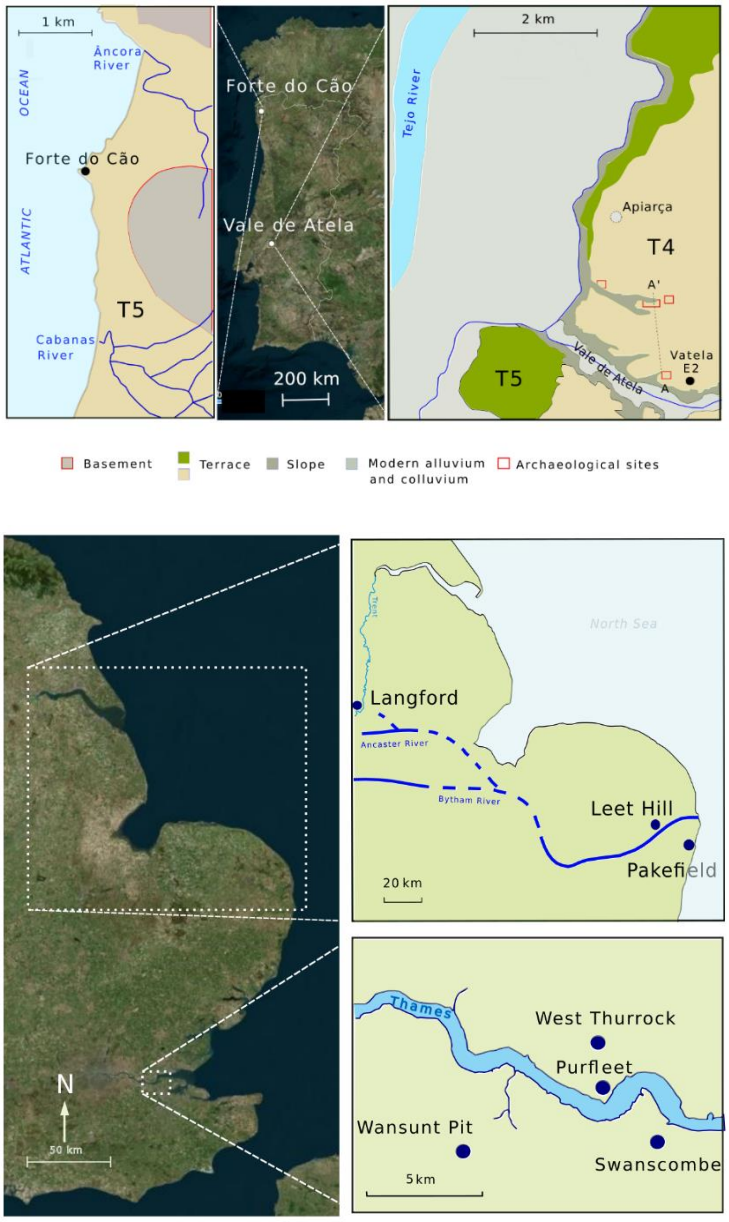

Figure 1

a) Map of western Iberia (centre) showing the locations in Portugal of the two sampling sites, Forte do Cão (LHS) and Vale de Atela (RHS, VAtela-E2), flanked by maps of their localities. As discussed in the main text, the sampled sites were set in terraces T5 (Forte do Cão) and T4 (Vale de Atela, VAtela-E2). The VAtela-E2 site is located within a region containing a number of important Palaeolithic archaeological sites. The central image is from Bing Maps and the adjacent maps were redrawn in simplified form after Carvalhido et al., 2014 (LHS) and Cunha et al., 2017 (RHS).

b) Map of eastern Britain with delineated areas indicating the locations of Langford and Leet Hill quarry sites and Swanscombe (Skull site and Barnfield Pit), as identified in the accompanying maps (RHS), together with the courses indicated of the pre-Anglian rivers, the Bytham and the Ancaster (Upper) and the existing Thames River (RHS, lower). The location of important Quaternary sites where Palaeolithic artefacts have been recovered are also shown (Pakefield, West Thurrock, Wansunt Pit, and Purfleet). The central image is from Bing Maps and the adjacent maps were redrawn in simplified form after Bridgland et al. (2019).

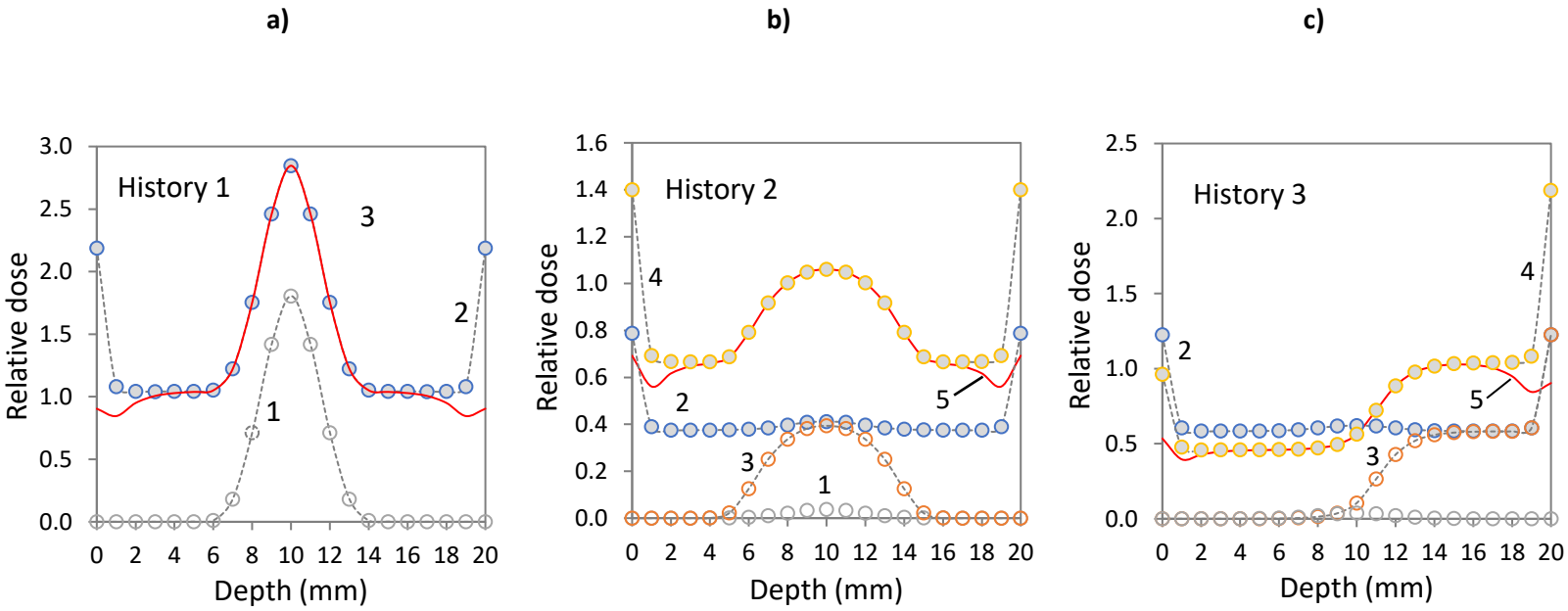

Figure 2
Calculated depth-dose profiles using a simplified optical bleaching model for a hypothetical lithic pebble in the form of a semi-infinite slab of 20 mm thickness, as discussed in the main text. The parameter values used to obtain the profiles are given and the details of each stage in each exposure and reburial history are given in Table 1.

a) Forte do Cão

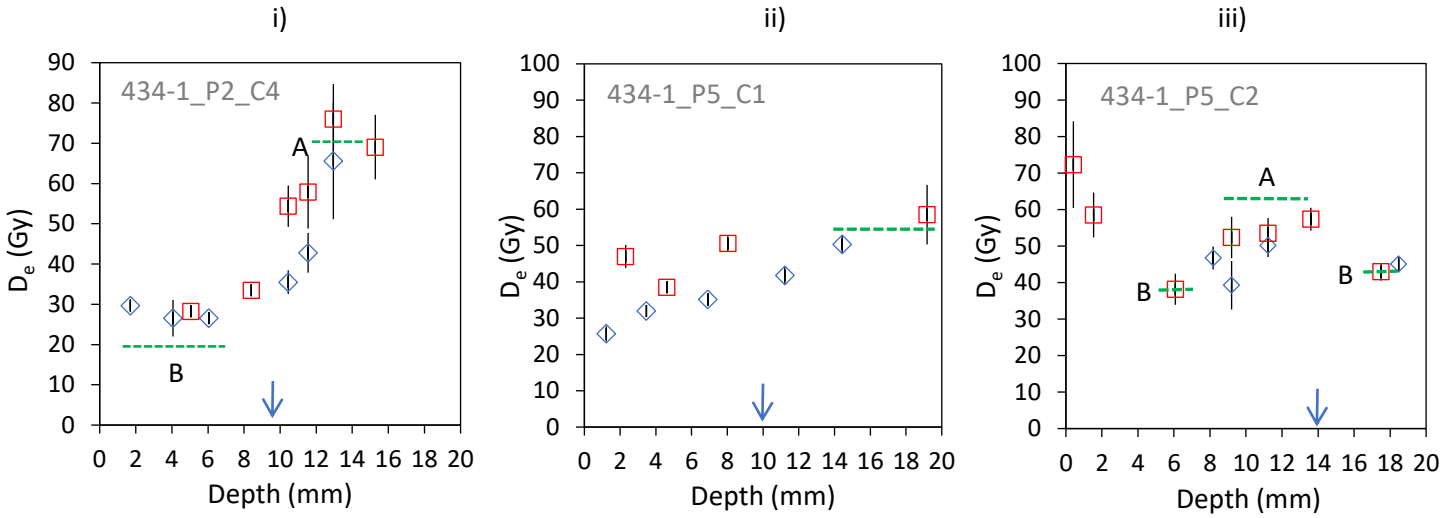

b) Vale de Atela

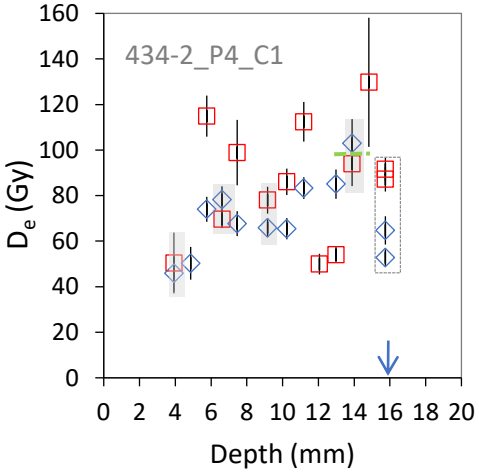

c) Swanscombe Skull Site and Barnfield Pit

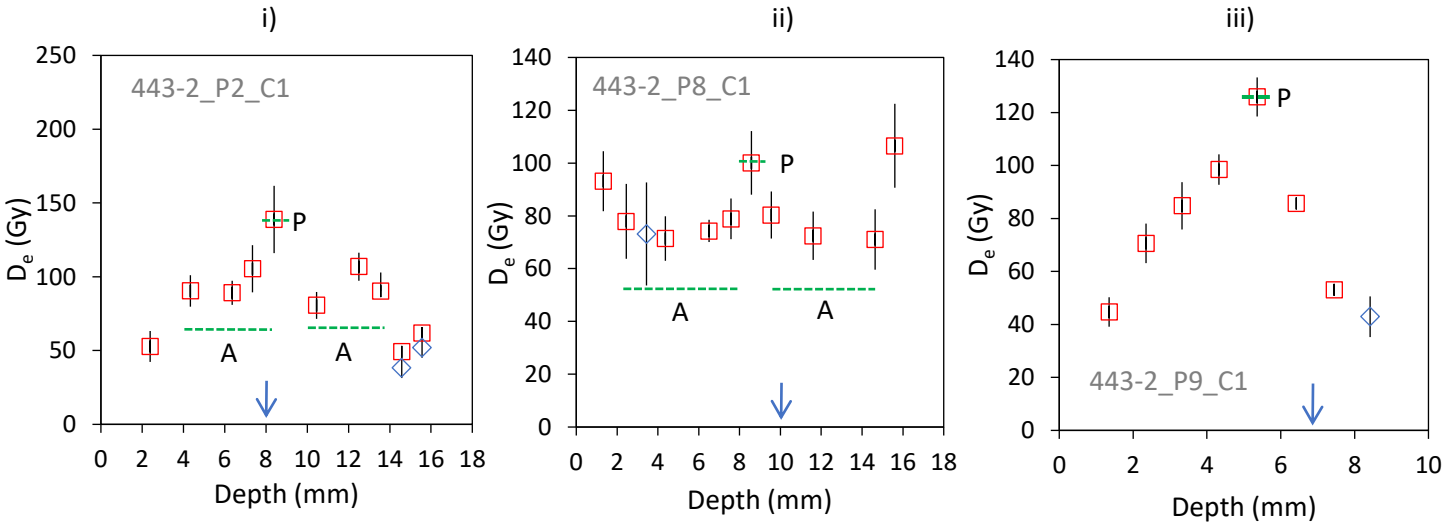

d) Leet Hill Quarry

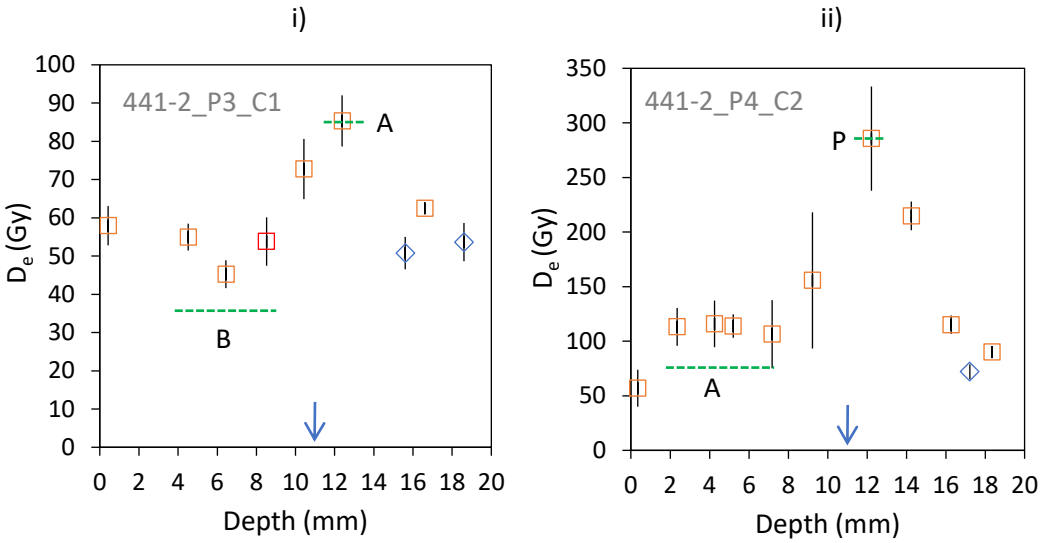

e) Langford Quarry

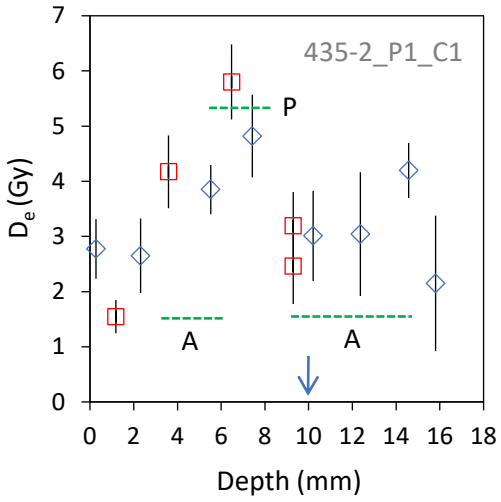

Figure 3
Experimentally determined depth-dose profiles obtained with cut slices, where the values of D_e are plotted against the central depth of the slice, starting from the surface of the pebble (depth = 0 mm) into which the core was cut. The D_e values plotted in these profiles were obtained using a SAR measurement procedure, employing either 240 °C (open diamonds) or 260 °C (open squares) preheat temperatures. For clarity, the slice thicknesses, discussed in the main text, are not plotted. The broken lines indicate single values or ranges within which one or more D_e values were averaged, denoted, with one exception (a(ii)), as either A, B or P, as discussed in the main text. The error bars represent the standard error (1σ) of the mean D_e value. The rectangular areas in b(i) are highlighted to aid discussion of the profile in the main text, and the vertical arrows pointing to the depth axis indicate the central region of the drilled section of pebble (but not necessarily coinciding with the central slice).

Supplementary Material. Document 1

Fieldwork

This document contains further details of the sampled sites and the chronological controls. For each site, the stratigraphic details provided that include i) sediment logs of sampled exposures and ii) their relationship to previously published sections. The sites include: a) the Forte do Cão outcrop, b) the Vale de Atela exposure, c) the Swanscombe Skull Site and Barnfield Pit exposures, d) the Leet Hill Quarry exposure, and e) the Langford Quarry exposure. The general key to the lithofacies and symbols is given below.

Lithofacies glossary and symbols

Abbrev.	Description	Abbrev.	Description
Fm	Fines, massive	Sc	Sand, steeply dipping planar cross bedding
Gm	Gravel, clast-supported, massive	Sh	Sand, horizontally laminated
Gms	Gravel, matrix-supported, massive	Sm	Sand, massive
Gp	Gravel, planar cross bedded	Sr	Sand, ripple-cross laminated
Gt	Gravel, trough cross-bedded	St	Sand, low angle crossbedding

Forte do Cão, Gelfa, Portugal

(Geographic location: 41°47'47.25" N -8°52'15.26" W)

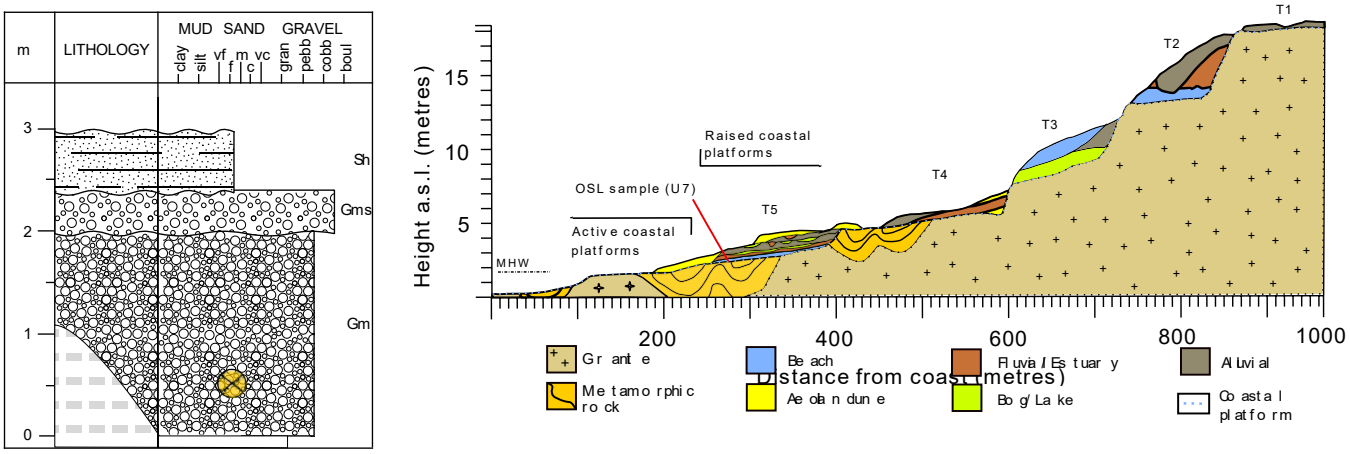

Figure SM1.1a

i) Sediment log of outcrop showing the location of the OSL sample.

ii) Profile showing the coastal terrace staircase (T1-T5) identified in the Minho-Neiva region, as discussed in the main text, where the horizontal axis is indicative only. The main facies are identified by colour coding; the location of the sampling site in the sedimentary unit U7 located at the base of terrace T5 and overlying the granite basement. (Adapted from Carvalhido et al., 2014).

At an elevation of 2.80 m above mean sea level (asl), the site lies just above the modern beach sands and gravels, at an elevation of c. 2.40 m asl, the marine basal deposits of the T5 terrace comprise (Fig. SM1.1a):

(i) an upper division, with a minimum thickness of 0.6 m, of fine aeolian white sand.

(ii) a middle division, with a thickness of 0.4 m, of angular boulder to pebble gravels of quartzite, with a matrix of fine sand (matrix-supported texture);

(iii) a lower division, with a maximum thickness of 2.0 m, of rounded pebble to cobble gravels, of quartzite and (milky) vein-quartz, in a matrix of medium sand (clast-supported texture); some clast imbrication can be identified.

Within the locality of this exposure, a sequence of five coastal terraces (Fig. SM1.1a(ii) was identified by Carvalhido et al. (2014) at the following elevations above modern sea level, comprising T1 - 20-18 m; T2 -13 m; T3 - 9.3-7.3 m; T4 - 5.5-4.5 m; T5 - 3.5-2.0 m, with sedimentary facies that are representative of coeval beach sediments in the lowest four. The OSL sample (Fig. SM1.1b) was taken from the gravel marine deposit in the T5 exposure. In their study, Carvalhido et al. (2014) applied luminescence techniques to coarse grained sand samples (250-180 μm) from terraces T2 and

T3, but obtained only minimum ages of 200 ka due to OSL signal saturation effects; terraces T4 and T5 were not sampled because the focus of the project on. On the basis of geomorphological position, terraces T5 and T4 are likely to correlate with MIS 7 and 5, respectively and the T5 sampled in this study is thus expected to have a burial age within the range 125-80 ka and, for the sample elevation given above, to have a depositional age of ~115 ka.

Figure SM1.1b *Forte do Cão, Gelfa, Portugal – sampled context with inset showing gravel concentration in a weathered exposure nearby*

Vale de Atela, Alpiarça, Portugal

(Geographic location: 39° 14' 01'' N -8° 34' 03'' W)

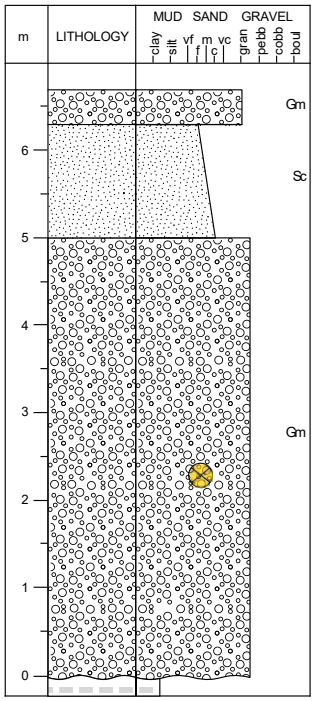

Figure SM1.2a
i) Sediment log of exposure showing the location of the OSL sample.

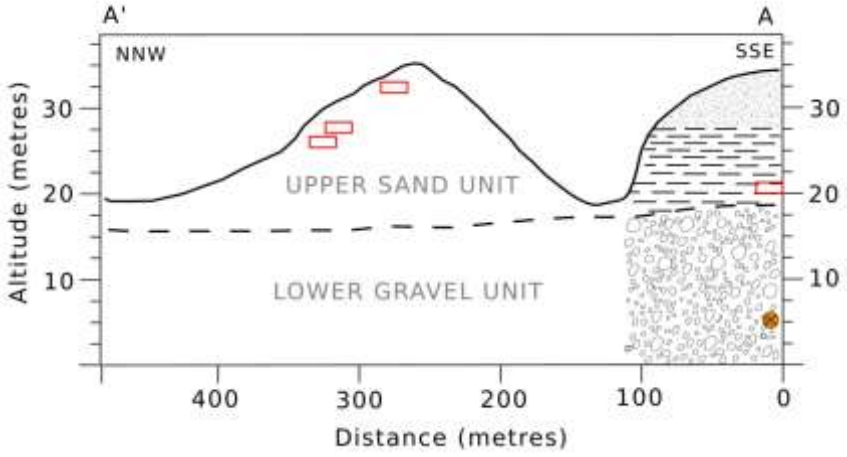

ii) Stratigraphic cross section (following NNW-SSE alignment A-A'; Fig. 1a) to the north of the River Tejo tributary valley Vale de Atela showing the landscape context of the sample site (VAtela-E2) and the locations of excavated Palaeolithic archaeological sites (open rectangles) within the Alpiarça area. (Adapted from Cunha et al., 2017).

The site (VAtela-E2) is located in the valley of the Atela stream, which is a tributary of the Lower River Tagus (Tejo), at an altitude of 32 m. In this reach of the Tagus valley there is a terrace staircase with six levels. Amongst these, T4, the fourth highest terrace, has a significantly wider outcrop and is formed by considerably thicker sediments than the other terraces (e.g., Mozzi et al., 2000; Cunha et al., 2017). Its sedimentary sequence also shows internal complexity, with lower gravelly and upper finer-grained divisions (Fig. SM1.2a(i)). The upper division (Upper Sands unit) has been dated by OSL to ~325–155 ka (Cunha et al., 2017) and the lower division (Lower Gravels unit) has a probable age of ~335–325 ka. The Vale de Atela easternmost site, which was sampled for this study, is a disused gravel pit that contains deposits of the T4 terrace similar to those present in the nearby site of Vale do Forno, where a series of important archaeological sites have been investigated (Fig. 1a, VAtela-E2 and Fig. SM1.2a(ii); Cunha et al., 2017). The OSL sample was collected ~2.7 m below the top of the Lower Gravels unit (Fig. SM1.2a; Fig. SM1.2b).

Figure SM1.2b *Vale de Atela, Alpiarça, Portugal - exposure (i) and sampled context (ii) showing cleaned exposure before full excavation of OSL sample (iii).*

Swanscombe Skull Site and Barnfield Pit, Kent, UK

(Geographic location: 51° 26′ 39.40″ N 000° 17′ 47.79″ E; Grid ref TQ 597 742)

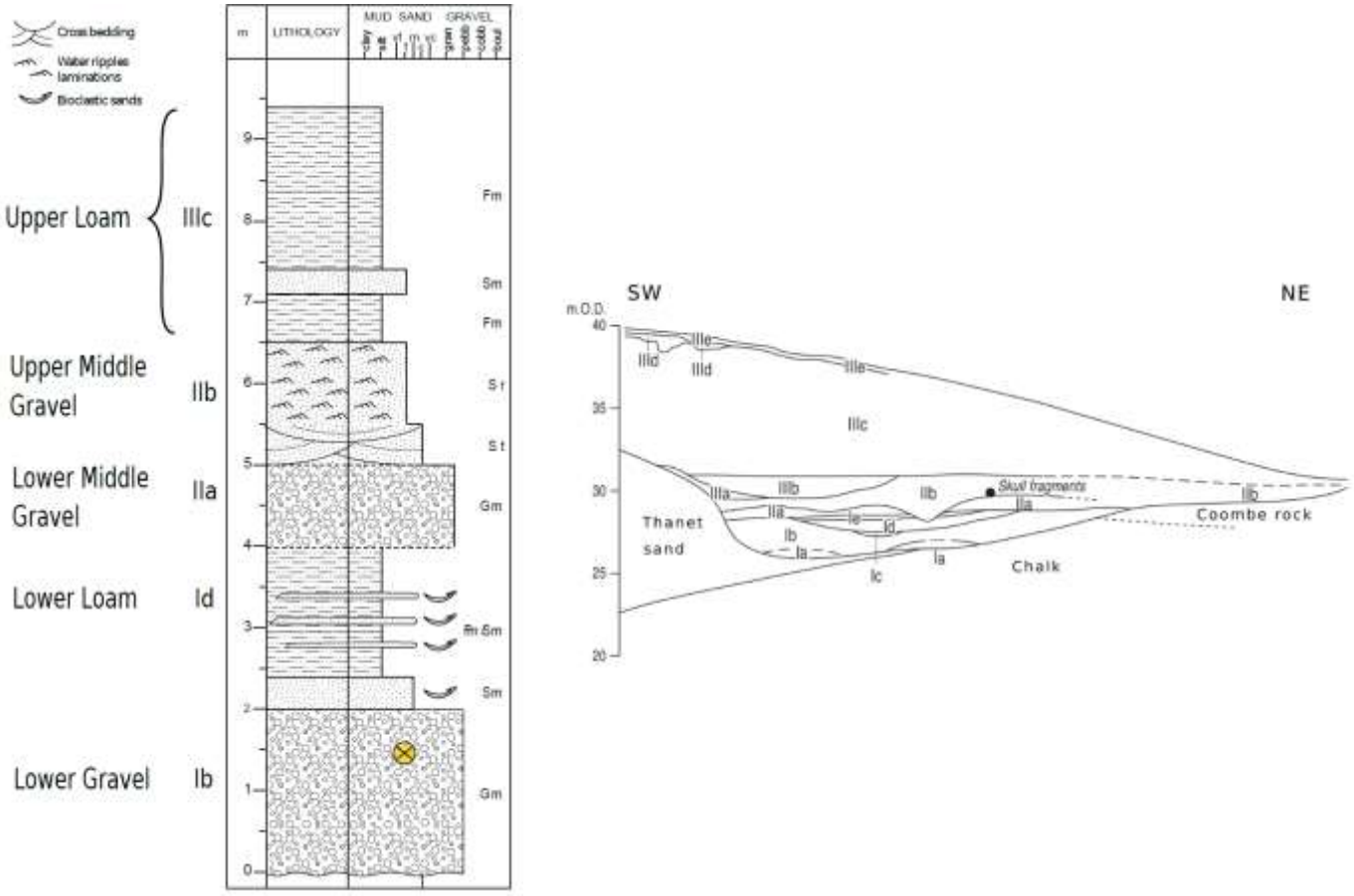

Figure SM1.3a

i) Sediment log of the exposure showing the location of the OSL sample in the lower gravel. The main units are linked (LHS) to the depositional phases shown in ii).

ii) A cross sectional transect of the Swanscombe sequence showing a phasing of deposits as presented by Bridgland et al. (2019), based on a combination of earlier work (Bridgland, 1994; Wenban-Smith and Bridgland, 2001). The ordinate values correspond to the elevation above OD.

The terrace deposits within the site record the oldest of the post-Anglian interglacials represented within the Lower Thames sedimentary succession (Conway, 1996). The upper division of the Lower Gravel deposits from Phase I of the sequence was accessed for sampling, within the upper 0.5 m of the deposit (Fig. SM1.3a(i)). The Swanscombe Lower Gravel unit comprises a coarse sandy horizontally-bedded gravel of up to 5 m thickness lying in a wide channel developed in underlying Palaeogene Thanet Sand. The archaeological evidence recovered from the Lower Loam overlying the Lower Gravel included lithic cores and flakes but lacked tools such as handaxes. On the basis of the similarity of the assemblage with those from other sites with Clactonian artefacts, in particular the

Clacton type locality (Bridgland et al., 1999), and the analysis of biostratigraphical evidence, the Phase I deposits are assigned to MIS 11c (White et al., 2013). The OSL sample (Fig. SM1.3b) was extracted from the upper 0.5 m of the Swanscombe Lower Gravel (Fig. SM1.3a(i)).

Figure SM1.3b *Swanscombe Skull Site and Barnfield Pit, Kent, UK - trench cut into slope to access the Lower Gravel unit, showing back-filled sample location following sampling; in situ measurement in progress using a portable gamma spectrometer.*

Leet Hill Quarry, Kirby Cane, Norfolk, UK

(Geographic location: 52° 28′ 59″ N 001° 30′ 18″ E; National Grid Reference TM 380 869 3044)

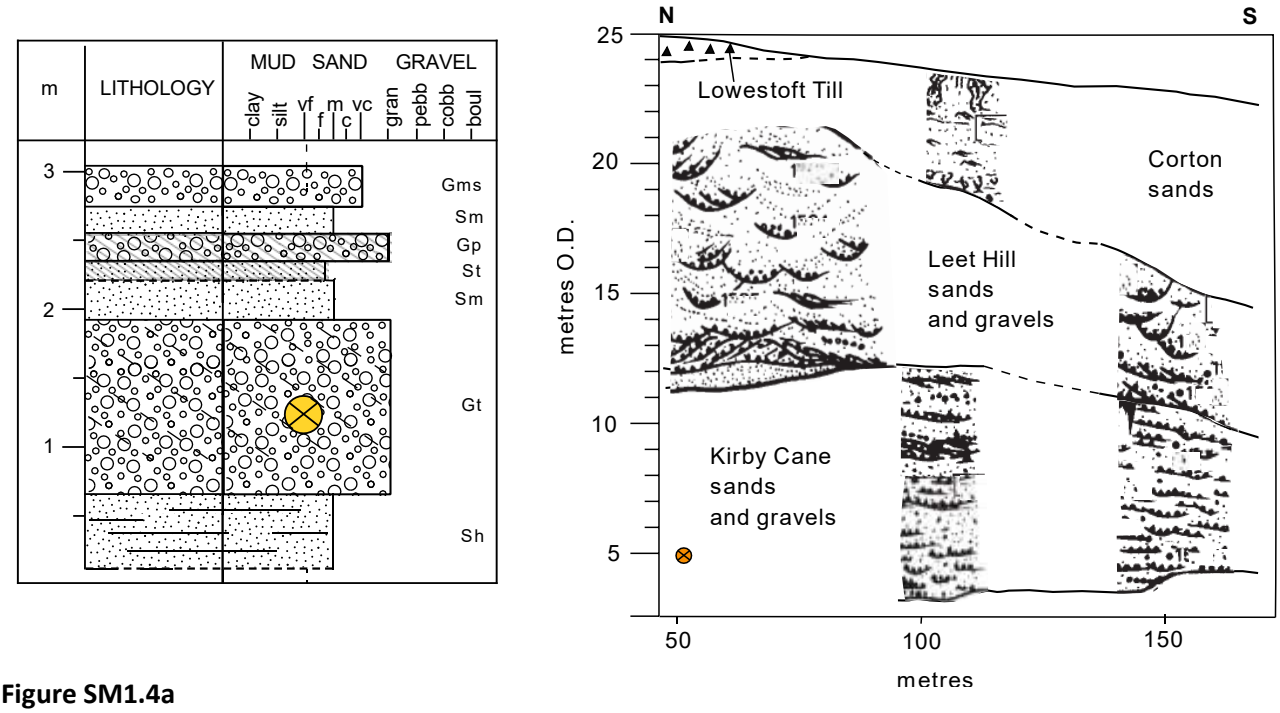

Figure SM1.4a

i) Sediment log of exposure showing the location of the OSL sample.

ii) Representation of sedimentary facies recorded at Leet Hill (redrawn from Rose et al., 1999). The ordinate values correspond to the elevation above OD.

The sequence of sands and gravels rising from the present floor of the quarry exposures (Fig 2d(ii) corresponds to the Kirby Cane and Leet Hill sands and gravels of Bytham River origin, passing upwards into the Corton Sands, which represent MIS 12 glacial outwash. The Kirby Cane sands and gravels are braided river deposits containing quartzite and vein-quartz clasts derived from the English Midlands, deposited under periglacial conditions (Lee et al., 2004). OSL samples were extracted within these deposits, assigned to early (pre-ice advance) MIS 12 (see Westaway, 2009), at the location indicated in Figs. SM1.4a(i), SM1.4a(ii) and SM1.4b. The overlying Leet Hill sands and gravel contain clasts, particularly of chalk, that indicate the input of glacial outwash into the Bytham, whereas the Corton Sands are regarded as glacio-fluvial in origin (SM1.4a(ii)). These uppermost gravels contain less Midlands material and reveal a switch in palaeocurrent direction from the eastward flow of the Bytham to a generally southward flowing glacial sandur aggradation overwhelming the Bytham valley (Rose et al., 1999; Lee et al., 2017). Confirmation of the Anglian glacial affinity of the sequence comes from the capping of Lowestoft Till (Rose et al., 1999). The age of the Kirby Cane sands and gravels has been controversial, having been assigned to MIS 16 as part of

the reinterpretation of the East Anglian Middle Pleistocene record known as the 'New Glacial Stratigraphy' (e.g., Hamblin et al., 2000, 2005; Preece et al., 2009). Detailed consideration of biostratigraphical evidence led Preece et al. (2009) to reject this new stratigraphy and to recognize only a single MIS 12 glaciation in the region, implying that the Kirby Cane sand and gravel would also date from MIS 12. Westaway (2009) concurred with this view, based on a reanalysis of the Bytham terrace sequence in East Anglia.

Figure SM1.4b *Leet Hill Quarry, Nottinghamshire, UK – (i) cleaned section in S-facing wall of quarry and (ii) sampled context with in situ measurement using a portable gamma spectrometer in progress.*

Langford Quarry, Newark, Nottinghamshire, UK

(Geographic location: 53° 07′ 57.58″ N 000° 46′ 33.01″ W; National Grid Reference SK 8200 6020)

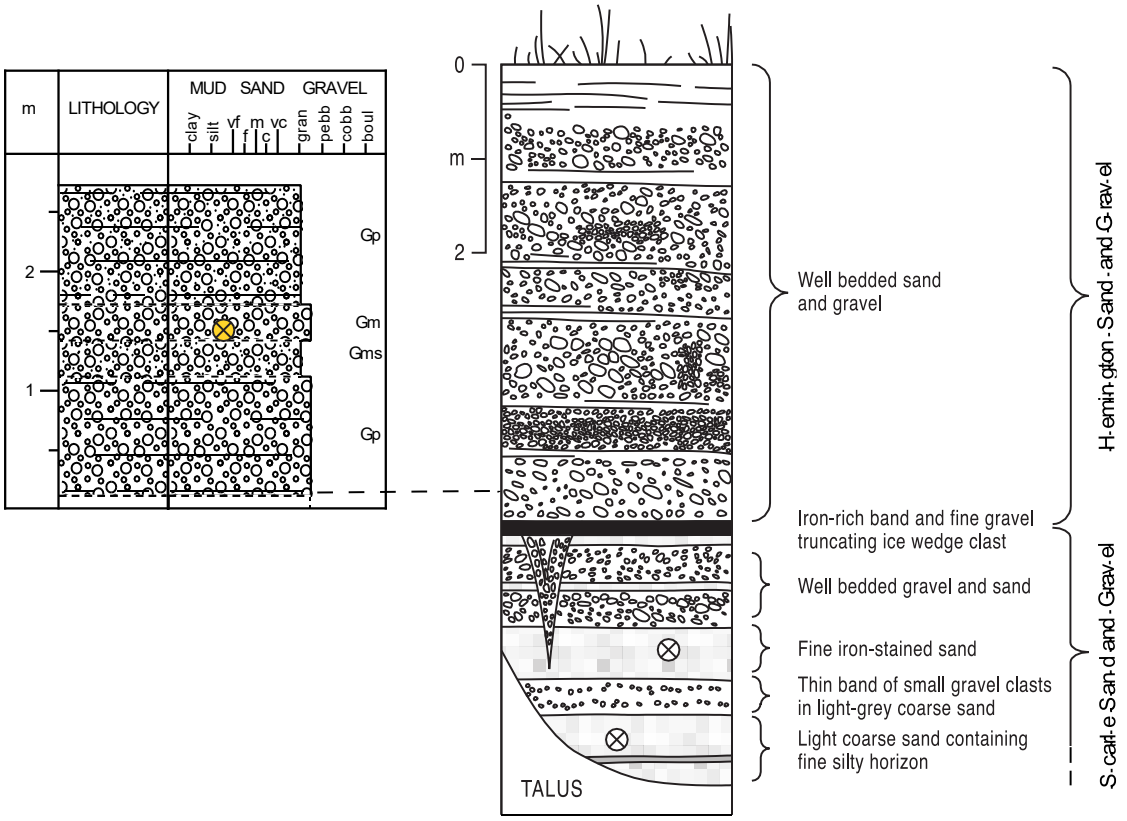

Figure.SM1.5a

i) Sediment log of exposure showing the location of the OSL sample.

ii) Full section at Langford Quarry. The section also shows the location of OSL samples for which burial ages (30.8 ± 3.3 ka and 27.9 ± 2.8 ka for upper and lower samples respectively) had been obtained in earlier work, as discussed in the main text. Adapted from Bridgland et al. (2014).

The upper part of the sequence at Langford Quarry (Fig. SM1.5a(i) and SM1.5b(ii)) is attributed to the Holocene Hemington Gravel Formation of the River Trent, which overlaps here onto gravels of the penultimate Pleistocene terrace of the river, the Scarle Sand and Gravel (Bridgland et al., 2014). The context from which the pebbles were sampled (Fig. SM1.5b) underlies the deposits that had yielded redeposited archaeological remains, as discussed in the main text. Earlier sections of the full sequence shown in the figure were no longer accessible within the quarry site and consequently could not be sampled. However, in earlier work, OSL dates were obtained for sands within the lower (Scarle Sand and Gravel) part of the sequence, from which ages of ~30 ka were obtained for the formation of ice-wedge pseudomorphs within the basal sands (Fig. SM1.5a(ii); Bridgland et al., 2014; Appendix 1). This mid–late Devensian age is in keeping with the conclusion that downcutting from the Scarle Terrace to the Holme Pierrepont Terrace, the latter being the lowest Pleistocene

Trent Terrace (formerly termed the 'floodplain terrace'), took place late in the Devensian Stage, during the Dimlington Stadial of MIS 2 (Bridgland et al., 2014).

Figure SM1.5b
Langford Quarry, Nottinghamshire, UK – Exposure (i), within which samples were extracted from the interior via the inserted pipe (iii). Indicated in (i) and (ii), sample 435-2 was extracted from a medium gravel unit.

Additional References

Bridgland, D.R., 1994. Quaternary of the Thames. Geological Conservation Review Series, 7, Chapman & Hall, London.

Bridgland, D.R., Field, M.H., Holmes, J.A., McNabb, J., Preece, R.C., Selby, I., Wymer, J.J., Boreham, S., Irving, B.G., Parfitt, S.A., Stuart, A.J., 1999. Middle Pleistocene interglacial Thames-Medway deposits at Clacton-on-Sea, England: Reconsideration of the biostratigraphical and environmental context of the type Clactonian Palaeolithic industry. Quaternary Science Reviews 18, 109–146.

Bridgland, D.R., Howard, A.J., White, M.J., White, T.S. (Eds), 2014. Quaternary of the Trent. Oxbow Books, Oxford. ISBN 978-1-78297-024-8

Bridgland, D.R., Briant, R.M., Allen, P., Brown, E.J., White, T.S., 2019. The Quaternary fluvial archives of the major English rivers: Field Guide. Quaternary Research Association, London.

Carvalhido, R.P., Pereira, D.I., Cunha, P., Buylaert, J.P., Murray, A.S. 2014. Characterization and dating of coastal deposits of NW Portugal (Minho–Neiva area): A record of climate, eustasy and crustal uplift during the Quaternary. Geology 328-329, 94-106. https://doi.org/10.1016/j.quaint.2014.01.025

Conway, B., 1996. The Stratigraphy and Chronology of the Pleistocene Deposits of Barnfield Pit, Swanscombe. *Excavations at Barnfield Pit, Swanscombe 1968-1972*. B. Conway, J. McNabb and N. M. Ashton. London, British Museum, 117-136.

Cunha, P.P., Martins, A.A., Buylaert, J.P., Murray, A.S., Raposo, L., Mozzi, P., Stokes, M., 2017. New data on the chronology of the Vale do Forno sedimentary sequence (Lower Tejo River terrace staircase) and its relevance as a fluvial archive of the Middle Pleistocene in western Iberia, Quaternary Science Reviews 166, 204-226. https://doi.org/10.1016/j.quascirev.2016.11.001

Hamblin, R.J.O., Moorlock, B.S.P., Rose, J., 2000. A new glacial stratigraphy for Eastern England. Quaternary Newsletter 92, 35–43.

Hamblin, R.J.O., Moorlock, B.S.P., Rose, J., Lee, J.R., Riding, J.B., Booth, S.J., Pawley, S.M., 2005. Revised Pre-Devensian glacial stratigraphy in Norfolk, England, based on mapping and till provenance. Netherlands Journal of Geosciences 84, 77–85.

Lee, J.R., Rose, J., Hamblin, R.J.O., Moorlock, B.S.P. 2004. Dating the earliest lowland glaciation of eastern England: a pre-MIS 12 early Middle Pleistocene Happisburgh glaciation. Quaternary Science Reviews 23, 1551–1566.

Lee, J.R., Phillips, E. Rose, J., Vaughan-Hirsch, D., 2017. The Middle Pleistocene glacial evolution of northern East Anglia, UK: a dynamic tectonostratigraphic–parasequence approach. Journal of Quaternary science 32, 231–260.

Preece, R. C., Parfitt, S. A., Coope, G. R., Penkman, K. E. H., Ponel, P., Whittaker, J. E., 2009. Biostratigraphic and aminostratigraphic constraints on the age of the Middle Pleistocene glacial succession in north Norfolk, UK. J. Quaternary Sci. 24 557–580. https://doi.org/10.1002/jqs.1245

Rose, J., Lee, J.A., Candy, I., Lewis, S.G., 1999. Early and Middle Pleistocene river systems in eastern England: evidence from Leet Hill. J Quaternary Science 14, 347-360.

Wenban-Smith, F.F., Bridgland, D.R., 2001. Palaeolithic archaeology at the Swan Valley Community School, Swanscombe, Kent. Proceedings of the Prehistoric Society 67, 219-225.

Westaway, R., 2009. Quaternary vertical crustal motion and drainage evolution in East Anglia and adjoining parts of southern England: chronology of the Ingham River terrace deposits. Boreas 38, 261–284.

White, T.S., Preece, R.C., Whittaker, J.E., 2013. Molluscan and ostracod successions from Dierden's Pit, Swanscombe: insights into the fluvial history, sea-level record and human occupation of the Hoxnian Thames. Quaternary Science Reviews 70, 73–90.

Supplementary Material. Document 2

Lithics

1. Pebble Drawings

Forte do Cão 434-1_P2

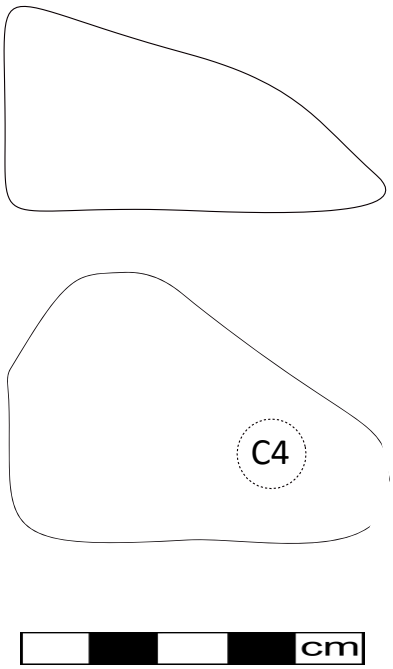

Forte do Cão 434-1_P5

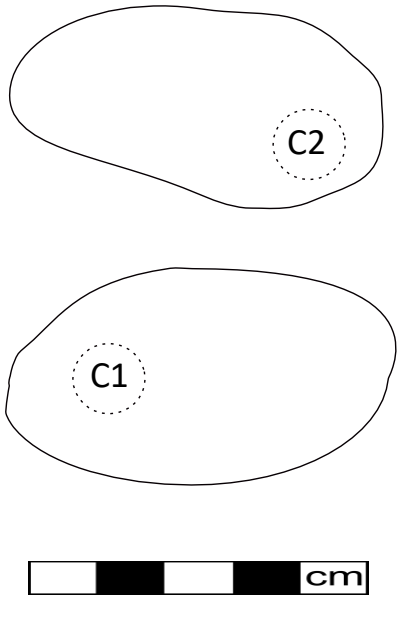

Vale de Atela 434-2_P4

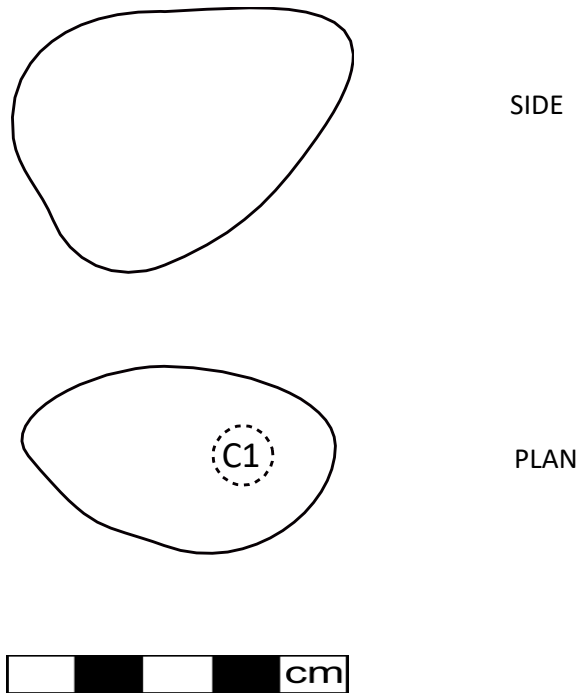

Langford 435-2_P1

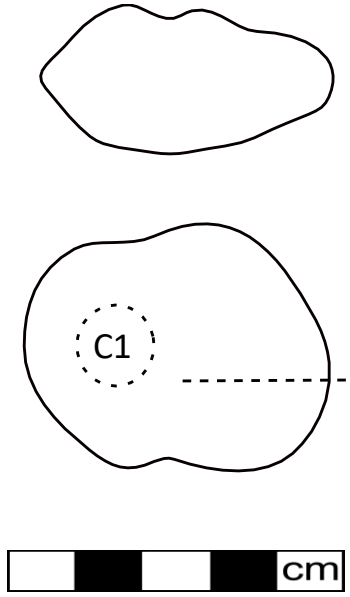

Leet Hill 441-2_P3

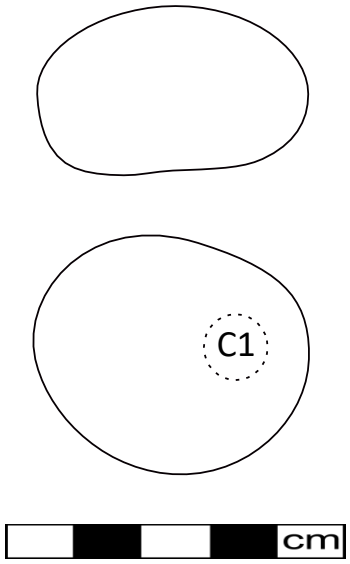

Leet Hill 441-2_P4

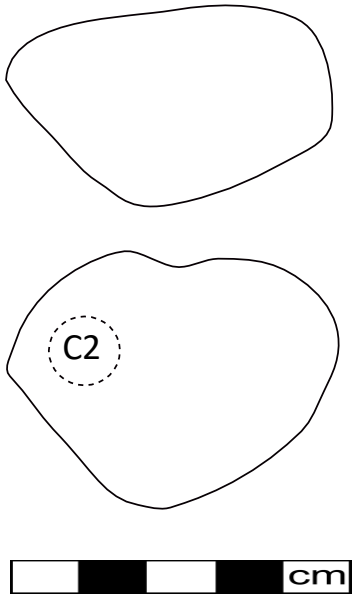

Swanscombe 443-2_P2

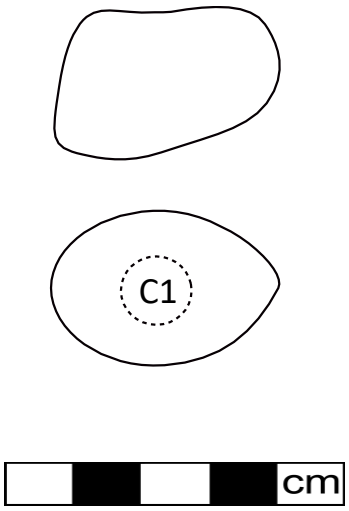

Swanscombe 443-2_P8

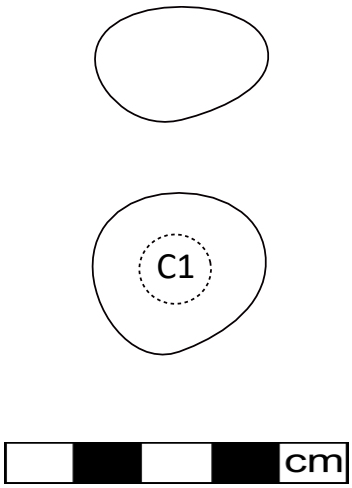

Swanscombe 443-2_ P9

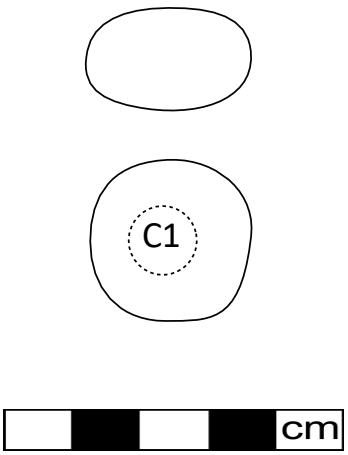

Figure SM2.1 Side and plan outlines of sampled pebbles, indicating the location of cores extracted for slicing and testing.

2. Slice Images

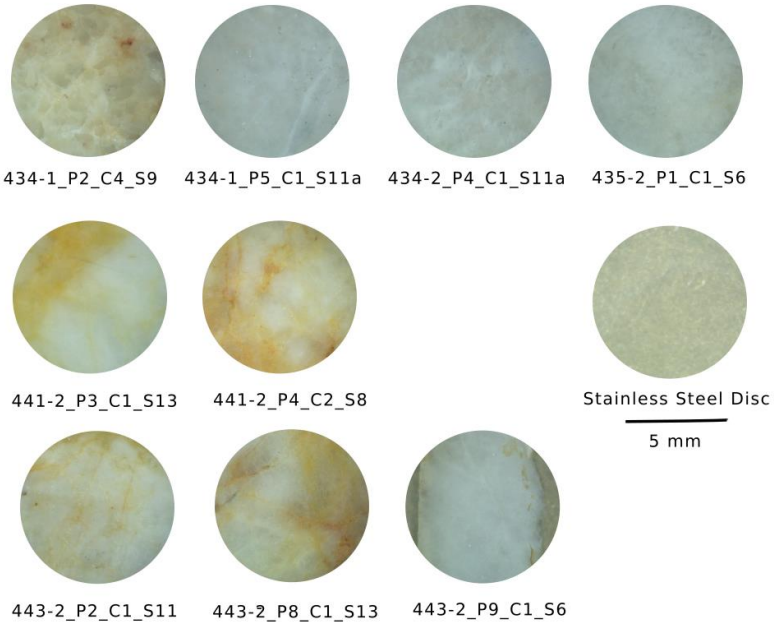

Figure SM2.2 Images obtained under fluorescent white light illumination of the surface of slices selected from each pebble core and placed on a stainless steel disc. The orange shading on a white/cream base coloration is associated with the presence of iron staining; relatively higher transparency was interpreted to be indicated by blue/green colouration (434-1_P5, 434-2_P4, 435-2_P1 and 443-2_P9) containing light reflected by the stainless steel disc. The images were obtained using a low power binocular microscope.

Supplementary Material. Document 3

Experimental

1. D_e evaluation

The single-aliquot regenerative dose (SAR) procedure applied to sliced samples is summarised in Table SM3.1. All OSL decay curve measurements (natural, regenerative and test dose) were performed at a sample temperature of 125 °C. The sensitivity-correct OSL signal was obtained by dividing the regenerative dose response by its immediately preceding test dose response.

Table SM3.1 Example of 4-point OSL single aliquot regenerative procedure

Step	Procedure	β dose	Measurement	OSL Signal
1	PH1; OSL		Pre-heat using a selected temp. within the range 240-280 °C; measure OSL	I_N
2	PH2; OSL		Pre-heat monitor (PHM)	I_{BG}
3	β1; PH1; OSL	β	1st dose point / Sensitivity Monitor	$I_{\beta 1}$
4	PH2; OSL		PHM	I_{BG}
5	β2; PH1; OSL	1.5β	2nd dose point	$I_{\beta 2}$
6	PH2; OSL		PHM	I_{BG}
7	β3; PH1; OSL	β	Sensitivity Monitor	$I_{\beta 3}$
8	PH2; OSL		PHM	I_{BG}
9	β4; PH1; OSL	3β	3rd dose point	$I_{\beta 4}$
10	PH2; OSL		PHM	I_{BG}
11	β5; PH1; OSL	β	Sensitivity Monitor	$I_{\beta 5}$
12	PH2; OSL		PHM	I_{BG}
13	β6; PH1; OSL	4β	4th dose point	$I_{\beta 6}$
14	PH2; OSL		PHM	I_{BG}
15	β7; PH1; OSL	β	Sensitivity Monitor	$I_{\beta 7}$
16	PH2; OSL		PHM	I_{BG}
17	β8; PH1; OSL	1.5β	Repeat ß2/Recycling test	$I_{\beta 8}$
18	PH2; OSL		PHM	I_{BG}
19	β9; PH1; IRSL; OSL	β	Sensitivity Monitor/Test for IR response	$I_{\beta 9}$
20	PH2; OSL		PHM	I_{BG}

Notes

1. The OSL decay curve was measured with the sample temperature held at 125 °C during the 20s stimulation period. The OSL signal corresponds to the cumulative photon counts recorded during the first 800 ms of stimulation.
2. The preheat PH1 was performed by heating the aliquot (5 ˚C s^{-1}) to a maximum temperature selected in the range 240-280 ˚C, recording the TL, holding at the maximum temperature for 5s, cooling to RT and then repeating the procedure. The preheat PH2 was performed by heating once to the maximum temperature as in PH1 and holding at that temperature for 10s; the signal recorded during the first 800 ms of stimulation is referred to as PBG.
3. βn represents the administration of a laboratory ß dose in the regenerative sequence, where Steps 3, 5, 7, 11 and 15 correspond to the monitor dose and where Steps 5 (β2), 9 (β4) and 13 (β6) correspond to the regenerative dose points respectively. The monitor dose was selected to be approximately equal to or slightly lower than the estimated burial dose ($\beta \cong D_e$).
4. The dose response curve was plotted using the OSL signal values, after subtraction of the background signal (I_{BG}), and normalisation to the preceding (except for I_N) sensitivity monitor as in the conventional SAR procedure, producing the following three sets of data pairs: 0, $I_N/I_{\beta 1}$; ß1, $I_{\beta 1}/I_{\beta 1}$; ß2, $I_{\beta 3}/I_{\beta 2}$; ß4, $I_{\beta 4}/I_{\beta 3}$; ß6, $I_{\beta 4}/I_{\beta 4}$ The recycling ratio was determined by evaluating the expression $(I_{\beta 8}/I_{\beta 7})/(I_{\beta 2}/I_{\beta 1})$; IR depletion was tested by examining the position of $I_{\beta 9}$ relative to the extrapolated trend line fitted to values of the sensitivity monitors, $I_{\beta 1}$, $I_{\beta 3}$, $I_{\beta 5}$, $I_{\beta 7}$, plotted against cumulative dose.
5. For the dose recovery experiment, the trapped charge was depleted at room temperature (RT) using the blue LED source and, following storage for 10 ks to deplete phototransferred charge in the traps associated with the 110 °C TL peak, any residual charge in the traps used for dosimetry was removed by a further OSL measurement at RT. Following this treatment, the applied dose, D_a, administered, selected to be approximately equivalent to the natural dose; followed by step 1 and subsequent measurements in the above procedure.

The second preheat (Step 2) and the subsequent OSL decay curve measurement (referred to as a pre-heat monitor, PHM) were included in the sequence to examine the OSL signal arising from thermal transfer, and also to define the background signal (PBG). During the first preheat for this pair of OSL measurements, the TL glow curve was recorded to monitor the position (reflecting thermal contact) and changes in sensitivity of the 110 °C TL peak. All OSL signals, including the background, PHM, used to construct the dose response characteristic were calculated as the summed counts recorded during the initial 800 ms of the OSL decay curve (channels 1-4).

Where the OSL signals were sufficiently strong, an early background (EBG) subtraction procedure (Ballarini et al, 2007; Cunningham and Wallinga, 2010) was also applied using signal integration intervals of 0-800 ms and 800-1600 ms for signal and background respectively. Comparison of D_e values calculated using EBG and PBG subtraction was used to assess the effect of intrusive medium and slow decay components (Li and Li, 2006; Steffen et al, 2009).

Representative examples of OSL decay curves obtained with a slice from each core shown in Fig. SM3.1 in pairs of: a) recorded photon counts plotted against stimulation time of the natural OSL (blue) and the following PHM background (red) using which the PBG signal was obtained and b) a plot of signals normalised to their initial value, where the PBG signal has been subtracted.

The OSL decay curve measured (under the same conditions as for the pebble slices) with a slice of quartzite distributed by the DTU Laboratory for the purposes of beta source calibration is shown on each normalised plot (broken black line) for comparison and also separately (Fig. SM3.1.1 1-10 a,b). The majority of decay curves recorded exhibited a dominant fast component. With one exception, the background signal, as plotted, was less than 100 counts/channel. In the case of the exception, Leet Hill Pebble 4 (441_2_P4_C2_S5), the background signal recorded during the PHM measurement was tenfold higher than the typical value observed with slices from the other cores (Fig. SM3.1 5a,b), forming an elevated signal that typically reduced by only ~10% during the 50 s stimulation period. However, this background signal could be reduced to typical levels after prolonged exposure (>1h) to an unfiltered 80 W medium pressure Hg lamp (4 mW cm^{-2} measured at the sample location; spectrum contained lines at 307, 364, 403, 434, 544 and 575 nm). The UV bleachable component is likely to be associated with deep traps in quartz (e.g., Jain, 2009). Although forming a much smaller proportion of the measured fast OSL component, a similar slowly decaying component was also observed in the measured OSL decay curve of the DTU quartzite slice (Fig. SM3.1 6a,b). For the purposes of the estimation of D_e, it was assumed that the PBG signal measured following the natural signal was representative of what would have been measured immediately after primary burial, adjusted for reduction during the preceding measurement of the natural OSL decay curve. The adjusted PBG signal, I_{BG}, was obtained by calculating a back-extrapolation of the PHM background signal to -50 s. This procedure was found to be equivalent to the extraction of the background signal associated with the slower decay component by curve fitting in a separate set of measurements with slices dosed to produce OSL signals of sufficient strength. For slices from this particular core (441_2_P4_C2), the adjusted PBG signal was ~8% higher than the measured value.

Rejection criteria

A series of SAR rejection criteria were applied to identify 'accepted' D_e determinations. Slices were rejected where the:

1) Total uncertainty in the test dose OSL response administered following the measurement of the natural OSL signal exceeded 20%;
2) Recycling ratio was not consistent with unity within 2σ limits;
3) Recuperation was greater than 5%;
4) IR-depletion ratio was smaller than unity by more than 2σ;
5) Natural sensitivity-corrected OSL response did not intersect the dose response curve;
6) The decay curves underwent a significant change in form following measurement of the natural OSL.

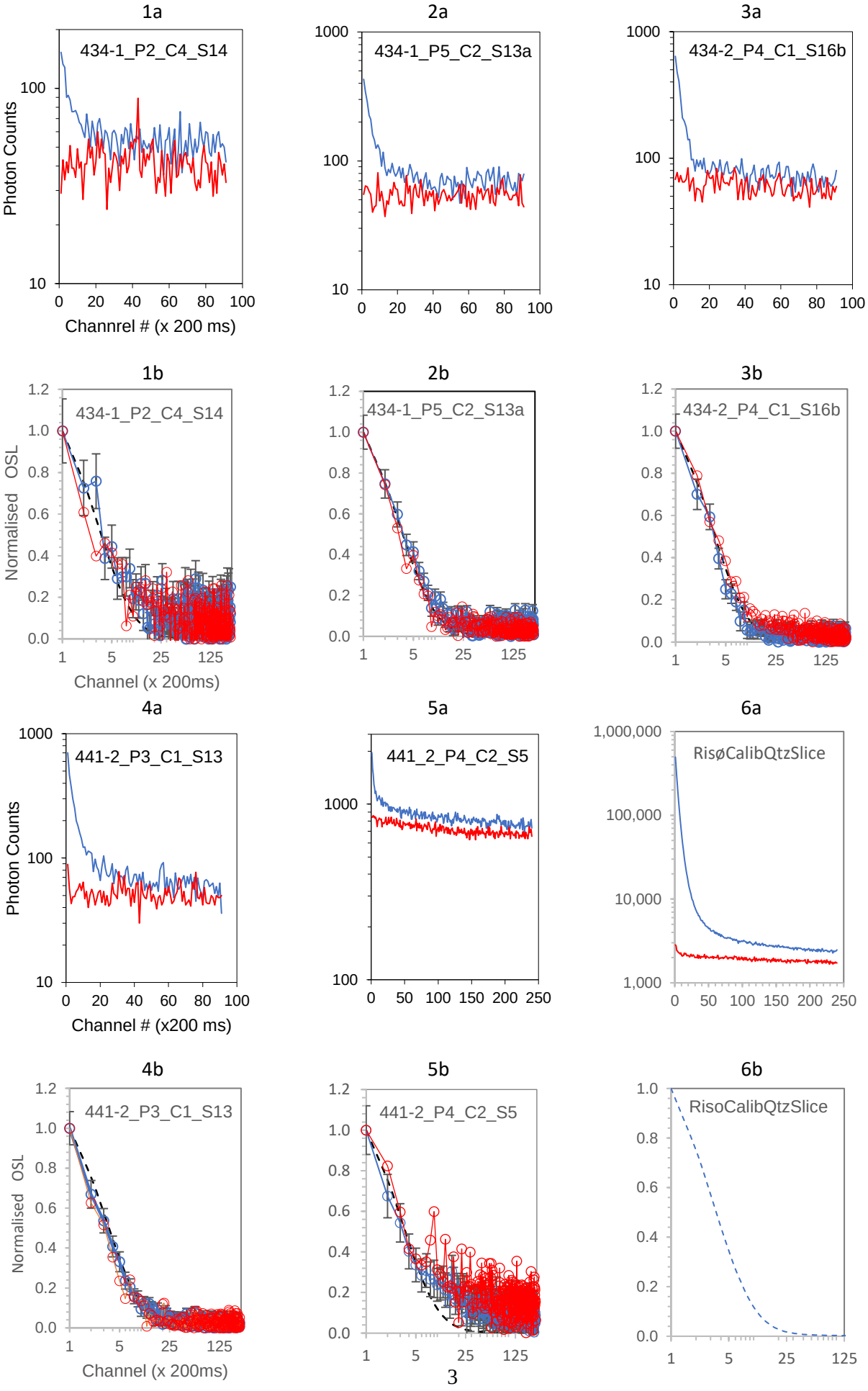
1a
434-1_P2_C4_S14
Photon Counts
Channrel # (x 200 ms)
2a
434-1_P5_C2_S13a
3a
434-2_P4_C1_S16b
1b
434-1_P2_C4_S14
Normalised OSL
Channel (x 200ms)
2b
434-1_P5_C2_S13a
3b
434-2_P4_C1_S16b
4a
441-2_P3_C1_S13
Photon Counts
Channel # (x200 ms)
5a
441_2_P4_C2_S5
6a
RisøCalibQtzSlice
4b
441-2_P3_C1_S13
Normalised OSL
Channel (x 200ms)
5b
441-2_P4_C2_S5
6b
RisoCalibQtzSlice

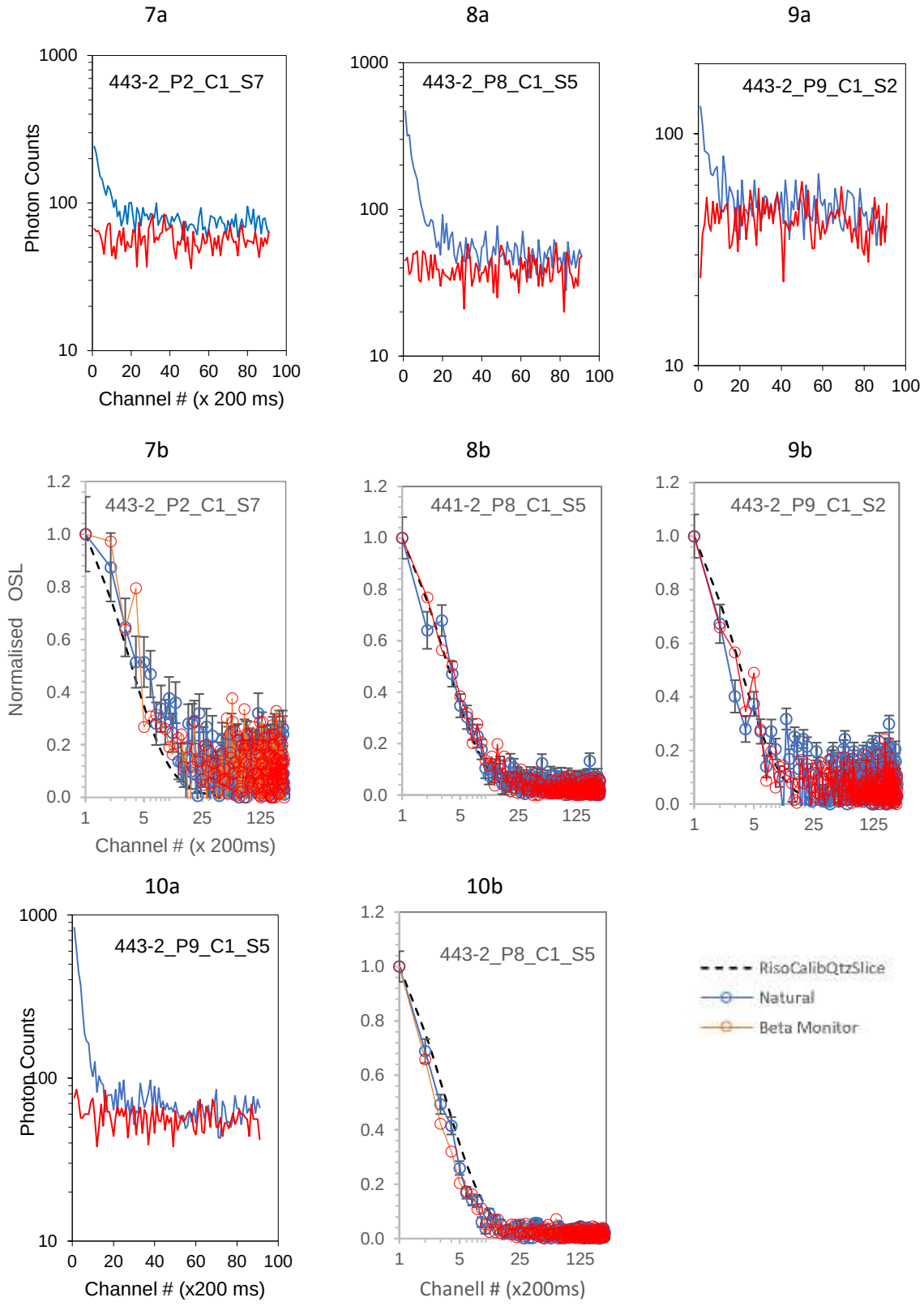

Figure SM3.1

Examples of a) natural (blue) and preheat background (red) OSL decay curves obtained with the slices indicated and b) normalised decay curves associated with the measurement of the natural OSL (blue), beta dose response (red) and DTU quartzite slice (black, broken). For clarity, only error bars associated *with the natural OSL signal are shown.*

OSL trap parameters - Isothermal decay

Estimates of the trap depth, E, and frequency factor, s, were obtained by performing storage experiments with a slice selected from each of 7 cores (Table SM3.2) following an isothermal decay measurement procedure similar to that described by Murray and Wintle (1999). As discussed above, the measured OSL decay curves exhibited a dominant fast component (Singarayer and Bailey, 2004). The measurement procedure followed is summarised in the table. A relatively large laboratory dose (~125 Gy) was applied to obtain sufficiently strong OSL signals following storage at elevated temperatures. A standard detection filter was employed (U-340). The OSL signal intensity corresponded to the integral of the first four counter channels (800 ms) and an 'early' background (integral of the following four channels) subtraction procedure was followed. As in the SAR procedure, the OSL signal of interest (step 4) was normalised by the OSL signal recorded following administration of the monitor β dose.

Following, Murray and Wintle (1999), the results of the isothermal decay measurements were plotted as logged values of the residual OSL, I, measured following storage at the indicated temperature, T, vs the storage period, t (s). From these plots, the decay constant, λ, was calculated by fitting to each set of data for a given storage temperature using the following single exponential function.

$$I = A \exp(-\lambda t) + \text{const.} \qquad \text{(SM3.1)}$$

Estimates of the trap depth, E (eV), and the frequency factor, S (s^{-1}), were obtained from an Arrhenius plot (example shown in Fig. SM3.2) of the logged values of the mean lifetime τ $(=1/\lambda)$ vs 1/kT, where T is the storage temperature (K) and k is the Boltzmann constant, where,

$$\tau = 1/\lambda = S^{-1} \exp(E/kT) \qquad \text{(SM3.2)}$$

A Monte Carlo simulation procedure was applied when fitting the exponential function to the Arrhenius plots to obtain estimates of uncertainty in E and S, and the values of s.d. are given to reflect the dispersion inherent in the calculations. The calculated values of E, S (as $\log_{10}S$) and mean lifetimes calculated for an average temperature of 20 °C are given in Table SM3.2.

Table SM3.2a Isothermal decay measurements

Step	Measurement		Preheat temp (°C)			
1	β dose (125 Gy)		260	270	280	290
2	Initial Preheat (260, 200 °C, 5s)		120	80	40	20
3	Elevated temperature storage (see RH table)	Storage	240	160	80	40
4	OSL (sample temp 125 °C), 50 s, 90% LED power	time (s)	500	350	160	60
5	Monitor β dose (~8 Gy)		1000	700	320	120
6	Preheat (180 °C, 5s); OSL as (4)					
7	Repeat (7); background measurement					

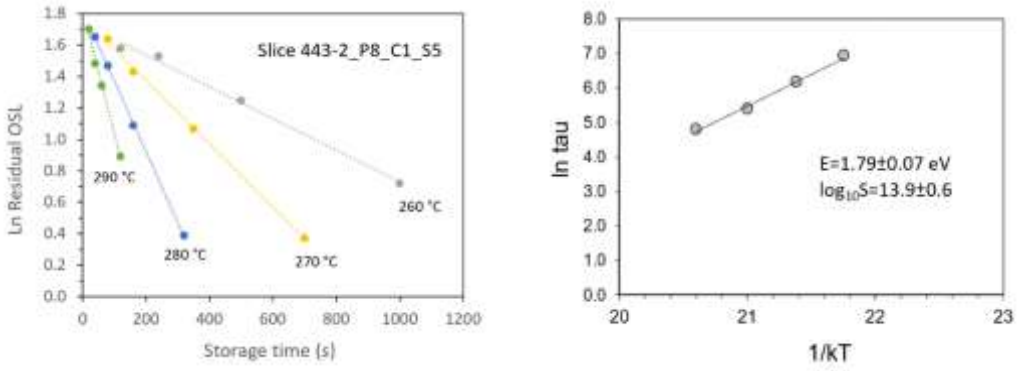

Figure SM3.2

Example plots of the results of a) isothermal storage at the temperatures indicated and b) an Arrhenius plot, as discussed in the main text.

Table SM3.2b Trap parameters obtained with selected core slices

Sample	E	$\log_{10}s$	τ (20°C)
	(eV)	(s^{-1})	(Ga)
Col.# (1)	(2)	(3)	(4)
Forte Cão			
434-1_P2_C4	2.04±0.09	14.5±1.1	254±21x10^3
_P5_C2	1.85±0.07	14.3±0.6	5.2±0.5
Vale de Atela			
434-2_P4_C1	1.84±0.08	14.7±0.7	7.2±1.1
Leet Hill			
441-2_P3_C1	2.03±0.08	15.9±0.7	467±92x10^3
P4_C2	1.89±0.12	14.5±1.1	22.4±5.9
Swanscombe			
443-2_P2_C1	1.90±0.08	15.1±0.8	11.1±1.6
_P8_C1	1.79±0.07	13.9±0.6	2.5±0.2

Dose recovery experiment

In addition to the mean values of D_e/D_a shown in the main text (Table 2, col. 6), Fig. SM3.3 contains radial plots of the (unlogged) ratio values grouped by preheat temperature (240 and 260 °C). The cases of overdispersion do not appear to be associated with particular pebbles. The difference between the weighted central values of two distributions is marginal.

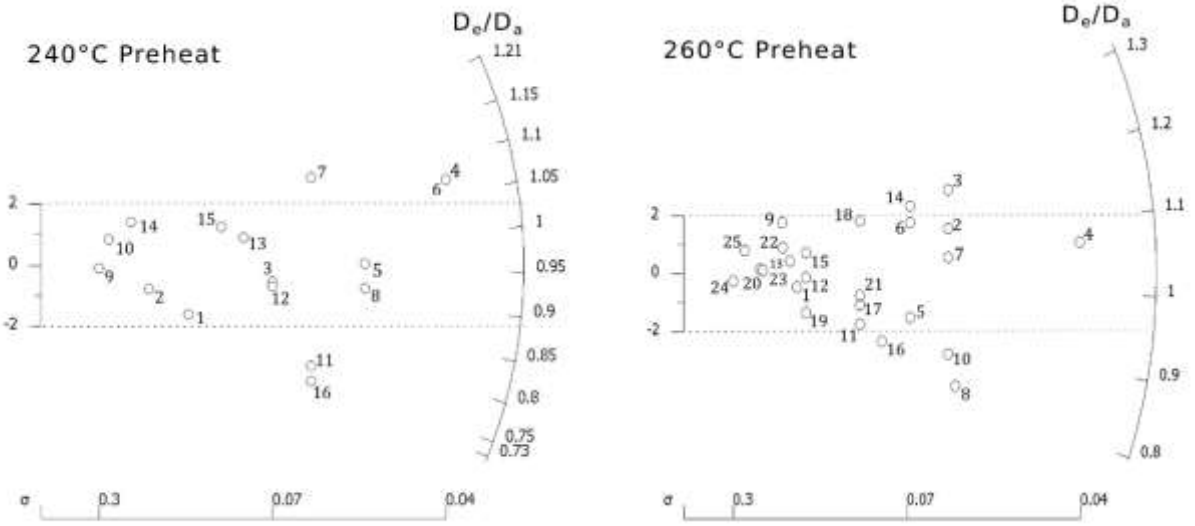

Central value=0.96±0.04 (n=16; OD=11%)

Central value=1.03±0.03 (n=25; OD=11%)

Key

Data points	Sample
[1-2]	434-1_P2_C4
[3-4]	434-1_P5_C1
[5-7]	434-1_P5_C2
[8-10]	434-2_P4_C1
[11-14]	435-2_P1_C1
[15]	441-2_P3_C1
[16]	441-2_P4_C2

Data points	Sample
[1-3]	434-1_P5_C2
[4-7]	434-1_P5_C1
[8-9]	434-1_P2_C4
[10-13]	434-2_P4_C1
[14 -15]	435-2_P1_C1
[16-18]	441-2_P3_C1
[19-20]	441-2_P4_C2
[21-22]	443-2_P2_C1
[23]	443-2_P8_C1
[24-25]	443-2_P9_C2

Figure SM3.3

Radial plots of D_a/D_e values obtained from the dose recovery experiments grouped by preheat temperature (240 and 260 °C), with the 2σ range indicated by broken lines. Each numbered data point represents a measurement slice, the key to which is given in the tabulated values. The weighted mean values (unlogged values) and standard errors, together with the overdispersion are given below the plots.

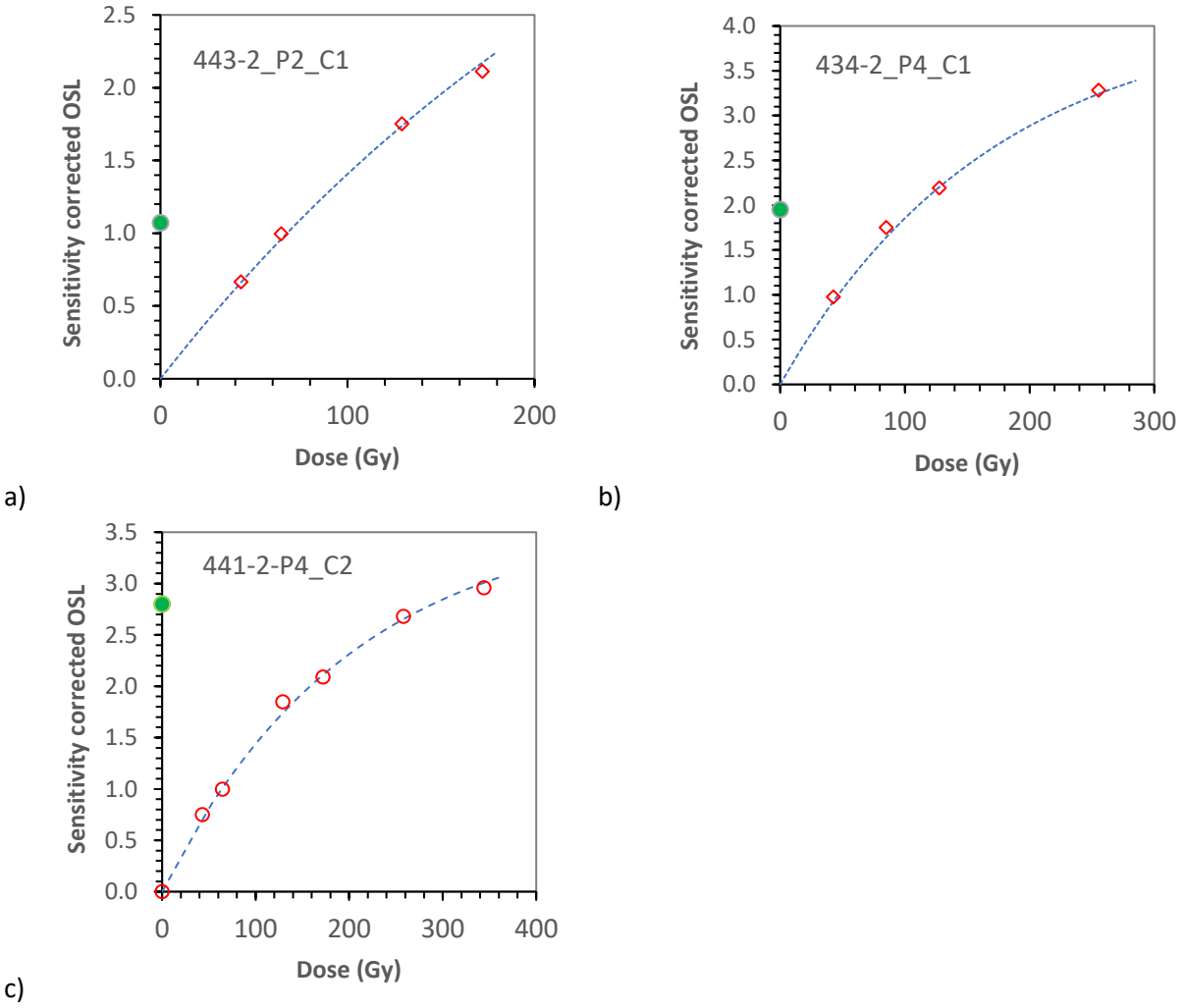

Figure SM3.4
Examples of SAR dose response characteristics obtained with pebble core slices from a) Swanscombe (443-2_P2_C1), b) Vale de Atela (434-2_P4_C1) and c) Leet Hill (441-2-P4_C2), where the filled circle plotted on the ordinate corresponds to the natural OSL signal. The broken lines represent a saturating exponential function fitted to the dose response values (open circles) using a Monte Carlo procedure.

A linear or single saturating exponential function was fitted to the sensitivity corrected dose response OSL data using a least squares algorithm, and the value of the burial dose, D_e, evaluated by interpolation. This fitting was repeated (>50 cycles) at each stage of a Monte Carlo (MC) simulation, where values of the OSL signal intensities were drawn from a normal distribution with a relative standard deviation derived from the (Poisson) uncertainty in the net integrated counts. The average value of the distribution of D_e values and its standard deviation obtained from the simulation provided an estimate of the equivalent dose, D_e. Values of OSL parameters including the natural: background signal, the recycling ratio and the dose characteristic, D_0, are listed in Table SM3.2.

$^{90}Sr/^{90}Y$ β source dose rate. The dose rate to sliced sample discs was determined following experiments with gamma irradiated slices and the application of radiation transport simulations (Bailiff, 2018) for the beta irradiator geometry. Forty slices that had been used for D_e evaluations and optically reset were exposed to a calibrated exposure of gamma radiation (^{60}Co, 20 TBq) at the Medical Research Council ^{60}Co Irradiation Facility, Harwell Campus, Didcot, Oxon; the absorbed dose was subsequently evaluated by applying the SAR procedure to each gamma irradiated slice. Radiation transport simulations (MCNP, Goorley et al, 2013) were performed to calculate a) the relationship between the dose in air and dose to quartz slices within the slice storage container (incorporating build-up material)

at the gamma source facility and b) adjustments to the $^{90}Sr/^{90}Y$ beta source dose rate according to slice diameter and thickness using an irradiation geometry similar to that developed earlier for the beta irradiator mounted on the luminescence reader (Bailiff, 2018). Using these calculations, for example, the source dose rate to an ~8.5 mm dia. slice was 7% larger than that to a 10.6 mm dia. slice, and that for an increase in slice thickness from 600 to 700 μm the dose rate is reduced by ~3%. On the basis of the calibration measurements, the average dose rate from the beta source to a slice of 10.6 mm dia. slice of 700 μm thickness was 2.8 Gy min^{-1} for the measurements discussed here.

2. Burial dose rate assessment

2.1 Beta and alpha dose rate - lithic interior

The radionuclide content of the lithics measured by ICP-MS is listed in Table SM3.3.

Table SM3.3 Analytical results: elemental concentrations in pebble slices measured using ICP-MS

Pebble Sample	^{238}U (ppb)	^{232}Th (ppb)	^{40}K (%)
434-1_P2	39	99	0.003
434-1_P5	5	30	n.d.
434-2_P4	110	65	0.002
435-2_P1	34	63	n.d.
441-2_P3	11	62	n.d.
441-2_P4	44	148	n.d.
443-2_P2	67	209	0.033
443-2_P8	8	25	n.d.

Notes. n.d. = not detectable

Table SM3.4 Specific activities of lithogenic radionuclides in burial medium sediment

Sample	^{238}U (Bq kg^{-1})	^{232}Th (Bq kg^{-1})	^{40}K (Bq kg^{-1})	$^{210}Pb/^{226}Ra$
434-1 Sediment	25.9±1.7	44.2±3.1	511±8	1.02±0.15
434-2 "	25.8±1.7	15.1±2.7	382±7	1.20±0.14
435-1 "	14.4±1.1	14.9±2.0	272±4	0.96±0.17
441-2 "	9.9±1.5	6.5±2.5	168±5	1.15±0.25
443-2 "	12.7±1.2	9.6±2.1	185±4	0.96±0.25

Notes. Measurements were performed using the high-resolution gamma spectrometer discussed in the main text. The sediment sample measured comprised a sub-granule sized (< 2 mm) fraction of the burial medium.

2.2 Beta dose rate - lithic sub-surface

A computational dosimetry model was constructed to simulate the beta dose rate delivered within the outer surface of a quartz pebble due to lithogenic radionuclides dispersed in the surrounding sediment and within the lithic materials. The general-purpose radiation transport code MCNP, version 6 (Monte Carlo N-particle Transport Code; Goorley et al, 2013) was used for the simulations. The number of particle history tallies registered was adjusted to obtain a precision of 1-2% in most cases, typically after 10^6-10^7 histories per simulation, but requiring up to 10^8 histories at large distances from the source volume. Some simulations were repeated with different random number generator starting values to check the consistency of the variation in the calculated dose coefficients

with the parameter uncertainty computed by MCNP. The beta particle energy spectra were obtained from the MIRD (Medical Internal Radiation Dose) database and the NUDAT 2 program (www.nndc.bnl.gov), and also included data from the RADAR database (www.doseinfo-radar.com), as discussed in Bailiff (2018).

A simple geometry was used in the model comprising a cylinder of 1 cm radius and length 2 cm divided into two along the major axis, one half of which comprised sediment and the other SiO_2. A series of *m* detector volumes were distributed along the major axis (1 mm dia. x 300 μm thick) in both sections of the cylinder, extending 4 mm into each half.

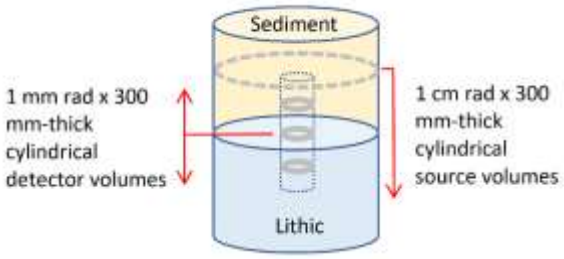

Figure SM3.5
Model geometry

The statistical parameter used as the basis of absorbed dose calculations is the *F8 tally, which corresponds to the average energy deposited (MeV) in the detector volume(s), E(*F8). The dose rate coefficient ${}_n\dot{D}_c^m$ (mGy a^{-1} per parent disintegration) for the m^{th} detector volume due to the n^{th} source volume of selected type (^{40}K, natural U or ^{232}Th) was calculated using expression SM3.3.

$$ {}_n\dot{D}_c^m = \frac{E(\,^*F8)}{m_D} \times C \times P_D, \qquad \text{(SM3.3)} $$

where m_D is the mass of the detector (g), C is a lumped scaling factor (5.0558) for energy and time units, P_D is the probability of decay per unit parent disintegration.

The average beta dose rate within the m^{th} detector volume due to the n^{th} source volume is given by,

$$ {}_n\dot{D}_\beta^m = {}_n\dot{D}_c^m \times A_P \times m_S, \qquad \text{(SM3.4)} $$

where A_P is the specific activity of the source (Bq g^{-1}) and m_S is the mass of the source within the source volume (g).

Following a similar approach to that taken in earlier work (Bailiff, 2018), a series of simulations were performed each with the sources uniformly distributed within one cylindrical volume of 1 cm radius and 300 μm thickness (Fig. SM3.5), calculating the energy deposited ($\dot{D}_c^m$) in each detector volume. The simulations were repeated with the position of the source volume incremented for each by 300 μm along the major axis from the upper surface within a) the section of cylinder containing the sediment and b) the section of cylinder containing the lithic. The dose rate in each of the detector volumes due to the n^{th} source volume was calculated using Eqn. SM3.4, and the average β dose rate to each detector volume obtained by summing the values of ${}_n\dot{D}_\beta^m$ for each of the source volumes contained within the sediment and lithic sections the cylinder. These calculations providing two dose rate profiles for sources located in each of the sections, with the other half being the inactive volume. These data were used to calculate, for a nominal concentration of each lithogenic radionuclide (^{40}K, natural U and ^{232}Th), the average dose rate within each detector volume, expressed as a percentage of the full energy release (FER) dose rate. The calculated average dose rate in two depth ranges containing the first two slices, S1 and S2, expressed as proportion of the

FER dose rate value of the linear are given in Table SM3.5. For comparison with other published data (Riedesel and Autzen, 2020), the values of the linear attenuation coefficient, b, calculated for each source type within a depth of 2 mm were 3.4, 2.0 and 2.3 mm^{-1} for K, nat. U and Th respectively.

Table SM3.5 Calculated dose rate depth reduction

Depth range (mm)	Average dose rate in depth range indicated due to external sources in sediment expressed as % of FER dose rate			
0-600	21	21	19	%
900-1500	1.0	3.4	2.3	%
	^{40}K	Nat.U	^{232}Th	

2.3 Gamma

In situ measurements of the gamma spectrum (typically >40 mins acquisition) were performed at each sampled context using a portable gamma ray spectrometer. Spectra were obtained using an (EG&G Ortec MicroNomad MCA coupled to a SCIONIX 76 x 76 mm Na(Tl) scintillation detector. The spectra were used to calculate the gamma dose rate following the 'threshold' approach (Mercier and Falguères, 2007) and where calibration of the instrument had been performed using the Oxford Laboratory calibration blocks (Rhodes and Schwenninger, 2007).

The specific activities of the ^{238}U and ^{232}Th decay chains and ^{40}K were measured using a high-resolution gamma-ray spectrometer. Sediment samples (< 2 mm dia.) extracted from the sampled context and excluding pebbles, were dried at 50 °C; a 25 g sub-sample of each was stored in a sealed container (with no other treatment) for at least 3 days to allow for the ingrowth of post-Rn daughters. Following storage, each sample was measured using a Canberra high purity germanium coaxial detector (GR2018) fitted with a carbon window and having 20% efficiency. The spectrometer had been activity calibrated using a series of certified silica-rich sands from New Brunswick Laboratories, USA and LGC Promochem and energy calibrated using a set of reference sources. The specific activities of U and Th are averages of six gamma emissions in the natural uranium decay chain (^{234}Th- ^{214}Bi) and nine in the thorium decay chain (^{228}Ac - ^{208}Tl).

2.4 Cosmic

The average cosmic dose rate during burial was calculated using a simplified model for the overburden with burial time based on an interpretation of the stratigraphy at each site, as discussed in the main text. The time-averaged cosmic dose rate was calculated using notional overburden profiles (Fig. SM3.6) for each site, taking into account major changes in sediment with time, and average densities of 1.6, 1.8 and 2.0 g cm^{-3} were assumed for sand or loam, gravel and debris respectively. These profiles are necessarily notional as a complete aggradation/erosional history is not available. In the case of Leet Hill, for example, the profile is based the existing stratigraphy as the depositional history following Anglian deglaciation is uncertain. If a further 10 m of sediment were added and subsequently eroded, the calculated time-averaged cosmic dose rate reduces by ~6 mGy ka^{-1}, which corresponds to a drop of ~3 % in the total dose rate in this case.

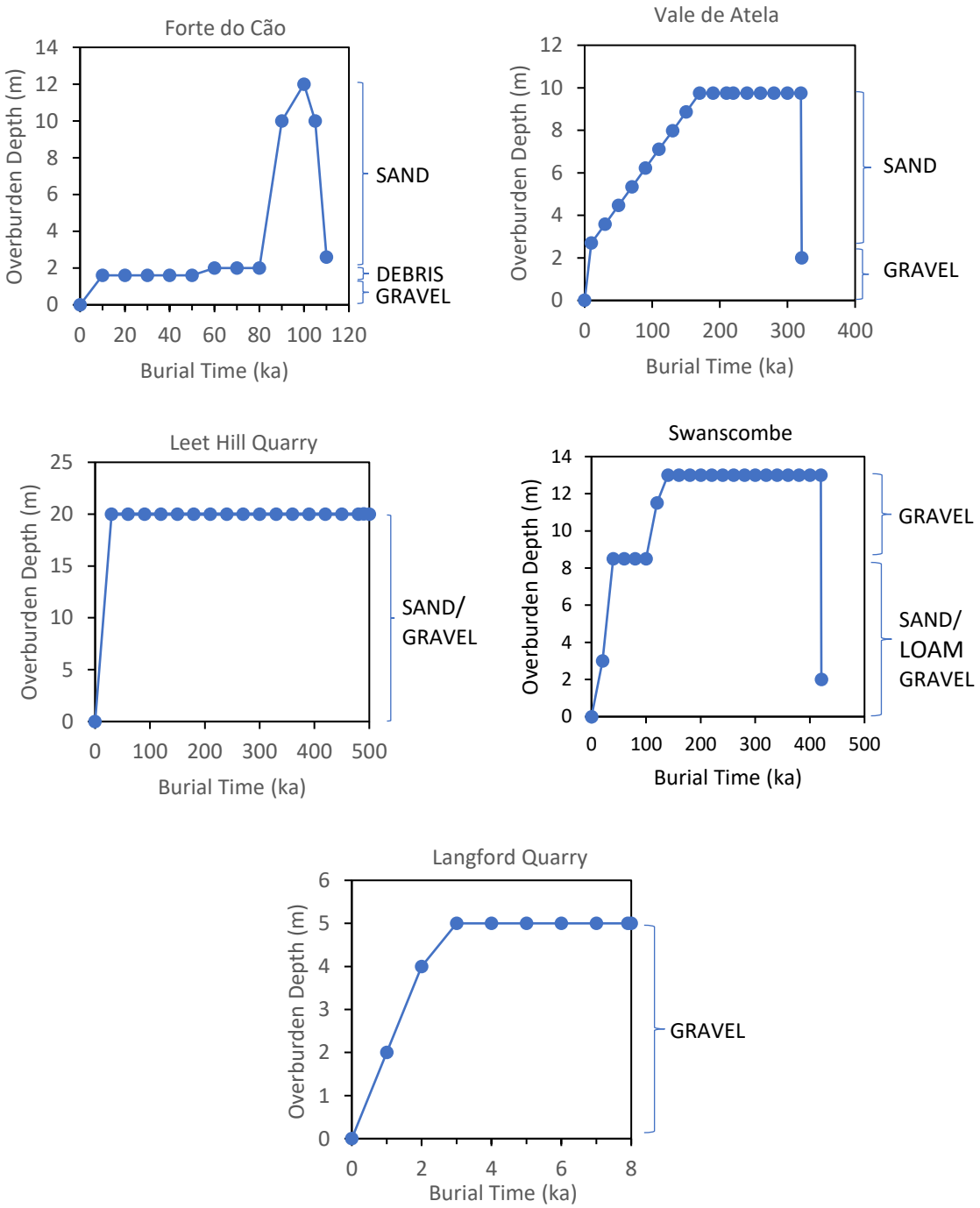

Figure SM3.6
Modelled overburden history profiles reflecting major changes in sediment with time.

Additional References

Bailiff, I.K., 2018. An examination of beta dose attenuation effects in coarse grains located in sliced samples. Radiation Measurements 120, 188-194. https://doi.org/10.1016/j.radmeas.2018.07.015

Ballarini, M., Wallinga, J., Wintle, A.G., Bos, A.J.J., 2007. A modified SAR protocol for optical dating of individual grains from young quartz samples. Radiation Measurements 42, 360-369. https://doi.org/10.1016/j.radmeas.2006.12.016

Cunningham, A.C., Wallinga, J., 2010. Selection of integration time intervals for quartz OSL decay curves. Quaternary Geochronology 5, 657-666. https://doi.org/10.1016/j.quageo.2010.08.004

Goorley, T., James, M., Booth, T., Brown, F., Bull, J., Cox, L.J., Durkee, J., Elson, J., Fensin, M., Forster, R.A., Hendricks, J., Hughes, H.G., Johns, R.B., Kiedrowski, R., Martz, Mashnik, S., McKinney, G., Pelowitz, D., Prael, R., Sweezy, J., Waters, L., Wilcox, T., Zukaitis, T., 2013. Initial MCNP6 release overview, MCNP6 version 1.0. LA-UR-11-05198. http://laws.lanl.gov/vhosts/mcnp.lanl.gov/pdf_files/la-ur-13-22934.pdf.

Guérin, G., Mercier, N., Adamiec, G., 2011. Dose-rate conversion factors: update, Ancient TL 29, 5-8.

Jain, M., 2009. Extending the dose range: Probing deep traps in quartz with 3.06 eV photons. Radiation Measurements 44, 445-452.

Li, B., Li, S-H., 2006. Comparison of D_e estimates using the fast component and the medium component of quartz OSL. Radiation Measurements 41, 125-136. https://doi.org/10.1016/j.radmeas.2005.06.037

Mercier, N., Falguères, C., 2007. Field gamma dose-rate measurement with a NaI(Tl) detector: re-evaluation of the "threshold" technique. Ancient TL 25, 1-4.

Murray, A.S., Wintle, A.G., 1999. Isothermal decay of optically stimulated luminescence in quartz. Radiation Measurements 30, 119-125.

Rhodes, E. and Schwenninger, J-L., 2007. Dose rates and radioisotope concentrations in the concrete calibration blocks at Oxford. Ancient TL, 25, 5-8.

Steffen, D., Preusser, F., Schlunegger, F., 2009. OSL quartz age underestimation due to unstable signal components. Quaternary Geochronology 4, 353-362. https://doi.org/10.1016/j.quageo.2009.05.015